

Transformations of galaxies in the environments of the cluster ABCG 209 at $z \sim 0.2$ [★]

A. Mercurio^{1,2}, G. Busarello¹, P. Merluzzi¹, F. La Barbera¹, M. Girardi², and C. P. Haines¹

¹ INAF - Osservatorio Astronomico di Capodimonte, via Moiariello 16, I-80131 Napoli, Italy

² Dipartimento di Astronomia, Università degli Studi di Trieste, Via Tiepolo 11, I-34100 Trieste, Italy

Received; accepted

Abstract. We analyse the properties of galaxy populations in the rich Abell cluster ABCG 209 at redshift $z \sim 0.21$, on the basis of spectral classification of 102 member galaxies. We take advantage of available structural parameters to study separately the properties of bulge-dominated and disk-dominated galaxies. The star formation histories of the cluster galaxy populations are investigated by using line strengths and the 4000 Å break, through a comparison to stellar population synthesis models. The dynamical properties of different spectral classes are examined in order to infer the past merging history of ABCG 209. The cluster is characterized by the presence of two components: an old galaxy population, formed very early ($z_f \gtrsim 3.5$), and a younger ($z_f \gtrsim 1.2$) population of infalling galaxies. We find evidence of a merger with an infalling group of galaxies occurred 3.5–4.5 Gyr ago. The correlation between the position of the young H δ -strong galaxies and the X-ray flux shows that the hot intracluster medium triggered a starburst in this galaxy population ~ 3 Gyr ago.

Key words. Galaxies: evolution — Galaxies: fundamental parameters (spectral indices, Sersic indices) — Galaxies: stellar content — Galaxies: clusters: individual: ABCG 209

1. Introduction

The influence of environment on the formation and the evolution of galaxies remains one of the most pressing issues in cosmology. The study of galaxy populations in rich clusters offers a unique opportunity to observe directly galaxy evolution, and environmental effects on star formation, by providing large numbers of galaxies at the same redshift which have been exposed to a wide variety of environments. In particular, galaxy populations in rich clusters are different from those in poorer environments, suggesting that some mechanism working on the cluster population is absent in the low density or field environments.

The first evidence for significant evolution in the dense environments of rich clusters over the past ~ 5 Gyr was the discovery of the Butcher-Oemler effect (Butcher & Oemler 1978, 1984), in which higher redshift clusters tend to have a larger fraction of blue galaxies than those at the present epoch (but see also La Barbera et al. 2003). This purely photometric result was subsequently confirmed through spectroscopic observations (e.g., Dressler & Gunn 1982, 1983, 1992; Lavery & Henry 1986; Couch & Sharples 1987), which have provided key information concerning the nature of blue galaxies, showing that several of them have strong emission line spectra, generally due to the presence of active star formation. They have also shown the existence of a class of galaxies, first identified by Dressler & Gunn (1983), which exhibit strong Balmer absorption lines without detectable emissions. Dressler & Gunn inferred the presence of a substantial population of A-type stars in these galaxies and concluded that a fraction of distant blue populations are “post-starburst” galaxies with abruptly truncated star formation. In this scenario, however, the most surprising result is that many red galaxies exhibit post-starburst spectra, indicative of a recent enhancement of star formation (e.g. Couch & Sharples 1987; Dressler & Gunn 1992).

Numerous studies have since been made to understand the evolution of these galaxies and the connection with the galaxy populations observed in clusters today (e.g. Couch & Sharples 1987; Barger et al. 1996; Couch et al. 1994; Abraham et al. 1996; Morris et al. 1998; Poggianti et al. 1999; Balogh et al. 1999; Ellingson et al. 2001). The emerging picture is that of a galaxy population formed early ($z \gtrsim 2$) in the cluster’s history, having characteristically strong 4000 Å breaks and red colours. Then the clusters grow by infall of field galaxies. This accretion process causes the truncation of star formation, possibly with an associated

Send offprint requests to: A. Mercurio

[★] Based on observations collected at the European Southern Observatory, Chile (Proposal ESO NM-0 68.AB-0116)

starburst. As this transformation proceeds, these galaxies might be identified with normal looking spirals, then as galaxies with strong Balmer absorption spectra, and finally as S0 galaxies, which have retained some of their disk structure but have ceased active star formation (Dressler et al. 1997).

On the other hand, there is observational evidence for a strong connection between galaxy properties and the presence of substructures, which indicates that cluster merger phenomena are still ongoing. Caldwell et al. (1993) and Caldwell & Rose (1997) found that post-starburst galaxies are located preferentially near a secondary peak in the X-ray emission of the Coma cluster and suggested that merging between Coma and a group of galaxies plays a vital role in triggering a secondary starburst in galaxies (but see also Goto et al. 2003a, 2003b).

Numerical simulations have shown that cluster mergers may trigger starbursts, and can affect greatly star formation histories. Tomita et al. (1996) argued that in a merging cluster some galaxies may experience a rapid increase of external pressure, passing through regions which are overdense in intra-cluster gas, leading to a starburst. An excess of star-forming galaxies is expected in the regions between the colliding sub-clusters. As shown by Bekki (1999), mergers induce a time-dependent tidal gravitational field that stimulates non-axisymmetric perturbations in disk galaxies, driving efficient transfer of gas to the central region, and finally triggering a secondary starburst in the central part of these galaxies. Roettiger et al. (1996) showed that during cluster-cluster mergers a bow shock forms on the edges of infalling subclusters, that protects the gas-rich subcluster galaxies from ram pressure stripping. This protection fails at core crossing, and galaxies initiate a burst of star formation.

The above results show that episodes of star formation in cluster galaxies can be driven both by the accretion of field galaxies into the cluster and by cluster-cluster merging. In order to disentangle the two effects it is crucial to relate the star formation history of cluster galaxies to global properties of clusters, such as mass and dynamical state.

To examine the effect of environment and dynamics on galaxy properties, in particular on star formation, we have performed a spectroscopic investigation of luminous galaxies in the galaxy cluster ABCG 209 at $z=0.21$ (Mercurio et al. 2003a and references therein) using EMMI-NTT spectra. ABCG 209 is a rich (richness class $R=3$, Abell et al. 1989), X-ray luminous ($L_X=(0.1-2.4 \text{ keV}) \sim 2.7 \times 10^{45} h_{70}^{-2} \text{ erg s}^{-1}$, Ebeling et al. 1996; $T_X \sim 10 \text{ keV}$, Rizza et al. 1998), and massive cluster ($M(< R_{\text{vir}}) = 2.25^{+0.63}_{-0.65} \times 10^{15} h^{-1} M_{\odot}$, Mercurio et al. 2003a). It is characterized by the presence of substructure, allowing the effect of cluster dynamics and evolution on the properties of its member galaxies to be examined. Evidence in favour of the cluster undergoing strong dynamical evolution is found in the form of a velocity gradient along a SE-NW axis, which is the same preferential direction found from the elongation in the spatial distribution of galaxies and of the X-ray flux as well as that of the cD galaxy, and in the presence of substructures. These substructures are manifest both in the elongation and asymmetry of the X-ray emission, with two main clumps (Rizza et al. 1998) and from the analysis of the velocity distribution (Mercurio et al. 2003a). Moreover, the young dynamical state of the cluster is indicated by the possible presence of a radio halo (Giovannini, Tordi & Feretti 1999), which has been suggested to be the result of a recent cluster merger, through the acceleration of relativistic particles by the merger shocks (Feretti 2002).

The data are presented in Sect. 2, and the spectroscopic measurement in Sect. 3. In Sect. 4 we discuss the spectral classification comparing data with models with different metallicities and star formation histories. We study separately the properties of disks and spheroids, on the basis of the Sersic index, in Sect. 5. We derive the age distribution of different spectral classes in Sect. 6. The analysis of the velocity distribution and of possible segregation is presented in Sect. 7. Finally we summarize and discuss the results in Sect. 8.

Throughout the paper, we use the convention that equivalent widths are positive for absorption lines and negative for emission lines.

We adopt a flat cosmology with $\Omega_M = 0.3$, $\Omega_{\Lambda} = 0.7$, and $H_0 = 70 h_{70} \text{ km s}^{-1} \text{ Mpc}^{-1}$. With this cosmological model, the age of the universe is 13.5 Gyr, and the look-back time at $z=0.21$ is 2.5 Gyr.

2. The data

The observations of the galaxy cluster ABCG 209 consist of spectroscopic and photometric data, collected at the ESO New Technology Telescope (NTT) with the ESO Multi Mode Instrument (EMMI) in October 2001, and archive Canada-France-Hawaii Telescope (CFHT) images.

Spectroscopic data have been obtained in the multi-object spectroscopy (MOS) mode of EMMI. Targets were randomly selected by using preliminary R-band images ($T_{\text{exp}}=180 \text{ s}$) to construct the multislit plates. A total of 112 cluster members with $R \lesssim 20.0$ were observed in four fields (field of view $5' \times 8.6'$), with different position angles on the sky. We exposed the masks with integration times from 0.75 to 3 hr with the EMMI-Grism#2, yielding a dispersion of $\sim 2.8 \text{ \AA}/\text{pix}$ and a resolution of $\sim 8 \text{ \AA}$ FWHM, in the spectral range 385 – 900 nm. Reduction procedures used for the spectroscopic data are described in Mercurio et al. (2003a). In order to perform the flux calibration, the spectrophotometric standard star LTT 7987 from Hamuy et al. (1994) was also observed.

The photometric data were collected on November 1999 (PI. J.-P. Kneib) using the CFH12K mosaic camera, consisting of B- and R-band wide field images, centred on the cluster ABCG 209 and covering a total field of view of $42' \times 28'$ ($8.6 \times 5.7 h_{70}^{-2} \text{ Mpc}^2$ at the cluster redshift). The CCDs have a pixel scale of 0.206 arcsec. The total exposure times for both B and R images were

Table 2. Wavelength ranges for equivalent widths of emission lines, expressed in Angstrom.

Name	Index bandpass	Blue continuum	Red continuum
[OII]	3713 – 3741	3653 – 3713	3741 – 3801
[OIII]	4997 – 5017	4872 – 4932	5050 – 5120
H $_{\alpha}$	6555 – 6575	6510 – 6540	6590 – 6620

The flux calibration was performed using observations of the spectrophotometric standard LTT 7987, whose spectrum was acquired before and after each scientific exposure. The sensitivity function, derived by using the tasks STANDARD and SENSFUNC (rms ~ 0.03), was applied to the galaxy spectra by using the task CALIBRATE. Within this task, the exposures are corrected for the atmospheric extinction, divided by the exposure time, and finally transformed using the sensitivity curve. The calibrated spectra were then corrected for the measured velocity dispersion by using DISPCOR.

In order to assess the quality of the flux calibration, we compared the V-R colours as derived from photometry (Mercurio et al. 2003b) with those measured from the spectra of 41 galaxies for which the observed wavelength range is greater than 4750–8750 Å. The resulting mean difference in colours turns out to be $\Delta(V-R) = 0.06 \pm 0.08$, proving that the derived fluxes are correct.

We measured the equivalent widths of the following atomic and molecular features: H $_{\delta A}$, H $_{\gamma A}$, Fe4531, H $_{\beta}$, Fe5015, Mg $_1$, Mg $_2$, Mg b , Fe5270, Fe5335. We adopted the definition of the extended Lick system (Worthey et al. 1994, Worthey & Ottaviani 1997; Trager et al. 1998), where the spectral indices are determined in terms of a central feature bandpass bracketed by two pseudo-continuum bandpasses at a resolution of ~ 9 Å FWHM, that is similar to ours². Following the convention, atomic indices are expressed in Angstroms of equivalent width, while molecular indices are expressed in magnitudes.

We also measured the equivalent widths for the emission lines [OII], [OIII] and H $_{\alpha}$ (see Table 2 for the definition of wavelength ranges), as well as the strength of the 4000 Å break $D_n(4000)$. We adopted the definition of $D_n(4000)$ by Balogh et al. (1999) as the ratio of the average flux in the narrow bands 3850–3950 and 4000–4100 Å. The original definition of this index by Bruzual (1983) uses wider bands (3750–3950 and 4050–4250 Å), and hence it is more sensitive to reddening effects.

The derivation of equivalent widths and the catalogue of spectroscopic measurements are presented in Appendix A.

4. Spectral classification

An useful tool to classify galaxies is the diagram of $D_n(4000)$ versus H $_{\delta}$ equivalent width (EW(H $_{\delta}$)) (or (B-R)-EW(H $_{\delta}$)); e.g. Couch & Sharples 1987, Barger et al. 1996) and the emission line measurements (e.g. [OII]). In this way galaxies can be divided in four classes: emission line (ELG), blue H $_{\delta}$ strong (HDS $_{\text{blue}}$), red H $_{\delta}$ strong (HDS $_{\text{red}}$) and passive (P) galaxies (see Fig. 1).

We remark that there is not a unique criterion in literature for the definition of spectral classes of galaxies, mainly because there is no general agreement on the definition of indices, and because the spectra vary in terms of S/N and resolution. Moreover, the comparison of spectral indices among different works is not straightforward since line indices are sensitive to the definition of the bands and to the method used to measure their strengths. Therefore, we derived spectral indices for both data and models with the same procedures and we used models themselves to define the spectral classes (see below).

4.1. Galaxy population models

To investigate the nature of galaxy populations in ABCG 209, we used the code GISSEL03 (Bruzual & Charlot 2003), by adopting a Salpeter (1955) initial mass function (IMF), with a stellar mass range from 0.1 to 100 M $_{\odot}$. Results vary only slightly choosing different IMFs (but maintaining the same mass range).

The GISSEL03 code allows the spectral evolution of stellar populations to be computed at a resolution of 3 Å (FWHM), with a sampling of 1 Å across the wavelength range 3200–9500 Å. Differently from previous models (Bruzual & Charlot 1993), this code provides galaxy spectra with different metallicities, in the range $Z = (0.005 - 2.5)Z_{\odot}$, which are required to break the age-metallicity degeneracy, through a comparison of age and metallicity sensitive indices (see Bruzual & Charlot 2003 for details).

Models were first degraded and resampled in order to match data and then $D_n(4000)$ and rest-frame equivalent widths were computed in the same manner as for observations. The free parameters in our analysis are the star formation rate and the age of the galaxies, while the adopted metallicities were $Z = 0.4Z_{\odot}$, Z_{\odot} , and $2.5Z_{\odot}$.

² The difference of 1 Å in resolution between our data and the extended Lick standard results in a difference in line indices amounting to about 1% of the uncertainty of the measurements.

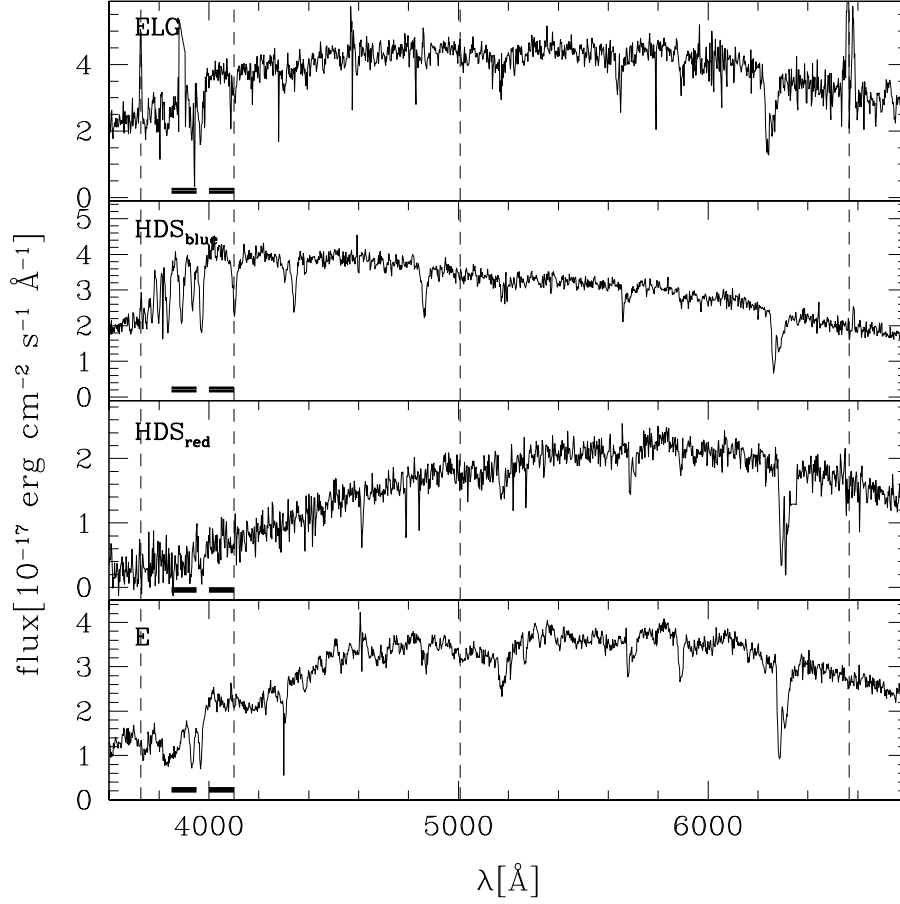


Fig. 1. Rest-frame spectra of galaxies belonging to different spectral classes. Lines [OII], H_δ , [OIII], H_α are highlighted by dashed lines. Wavelength ranges adopted to measure $D_n(4000)$ are also indicated by black lines.

4.2. Emission line galaxies

We define emission line galaxies as those showing in the spectra the emission lines [OII] and H_α significant at $\geq 1 \sigma$, and [OIII]. When the [OII] line is out of the observed wavelength range, we require [OIII] and H_α emission lines with $\geq 1 \sigma$ to define an emission line galaxy (see Table 4). We decided to use simultaneously these three lines and not only [OII], because i) we lack information on [OII] for more than half of spectra (because of the available wavelength range), ii) [OII] is heavily obscured by dust, and iii) [OII] is found at wavelengths where the noise is higher.

This class contains star-forming (SF) and short starburst (SSB) galaxies (Balogh et al. 1999). We interpret these as systems undergoing a star formation, that can be described by a model with exponentially decaying SFR model with decay parameter $\mu=0.01^3$ (Barger et al. 1996). SSB galaxies, on the contrary, have experienced a large increase of star formation over a short time, and can be described by models with an initial burst of 100 Myr.

We detect emission lines in $\sim 7\%$ of cluster members.

4.3. H_δ -strong galaxies

In order to investigate the physical properties of HDS galaxies, we divided the sample into blue and red galaxies, according to B-R colours corrected for the colour-magnitude (CM) relation: $(B-R)_{\text{corr}} = (B-R) - (3.867 - 0.0815 \cdot R)$. This relation is obtained by performing MonteCarlo realisations of the cluster populations, and fitting the resulting photometric data of $\sim 480 R < 21.0$ galaxies within one virial radius with the biweight algorithm (see Haines et al. 2004 for more details).

We define as “blue” the galaxies with rest-frame B-V colours at least 0.2 mag bluer than that of the CM relation, as for the original studies of Butcher & Oemler (1984). We estimate the corresponding change in B-R colour at the cluster redshift by firstly considering two model galaxies at $z = 0$ (Bruzual & Charlot 2003), one chosen to be a typical early-type galaxy 10 Gyr

³ $\mu=1-\exp(1.0 \text{ Gyr}/\tau)$

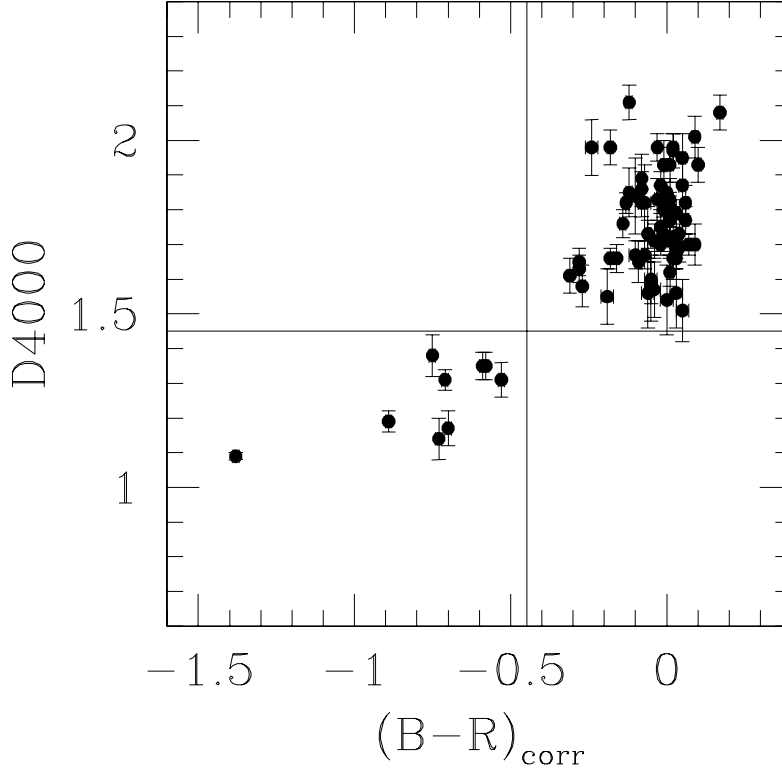


Fig. 2. Observed distribution of $D_n(4000)$ versus $(B-R)_{\text{corr}}$ (see text) for 76 member galaxies for which we can measure $D_n(4000)$. The vertical line indicates the separation between blue and red galaxies as defined in Haines et al. (2004) and the horizontal line is the cut for the break at 4000 \AA , adopted by Balogh et al. (1999).

old with solar metallicity, and the second reduced in age until its B-V colour becomes 0.2 magnitude bluer. After moving both galaxies to the cluster redshift, the difference in their observed B-R colour is found to be 0.447 mag (see Haines et al. 2004 for details). Thus we define as “blue” the galaxies with $(B-R)_{\text{corr}} < -0.447$.

The relation between $D_n(4000)$ and $(B-R)_{\text{corr}}$ (Fig. 2) shows that there is a clear separation between blue and red galaxies and that we can adopt $D_n(4000) = 1.45$ as a cut for the measurement of 4000 \AA break. This value corresponds to that adopted by Balogh et al. (1999), for the classification of galaxies in the CNOC sample.

In Fig. 3 we plot, in the $D_n(4000)$ – $\text{EW}(H_\delta)$ plane, the data (open circles) of 76 galaxies, for which we have information on both $D_n(4000)$ and H_δ , with superimposed the output of four different models: i) a model with an initial burst of star formation lasting 100 Myr (long dashed line); ii) a model with an exponentially decaying SFR with decay parameter $\mu=0.01$ (continuous line) lasting 11 Gyr and iii) truncated at 10 Gyr (dotted line); iv) a model with an exponentially decaying SFR with time scale $\tau = 1.0$ Gyr (short dashed line).

For blue galaxies, to reach $\text{EW}(H_\delta) > 5.0 \text{ \AA}$, the galaxy light must be dominated by A- and early F-type stars, whereas the presence of O- and B-type stars, which have weak intrinsic H_δ absorption, reduces this equivalent width. Moreover, the equivalent width of H_δ is inversely related to the duration of star formation. For this reason, the blue, H_δ -strong galaxies are expected to be the result of a short starburst or of a recently terminated star formation (e.g. Dressler & Gunn 1983; Barger et al. 1996). By using models i) and iii) above, with solar metallicity⁴, when $D_n(4000)$ is equal to 1.45, the H_δ equivalent width is 5.0 \AA , so we decided to use $\text{EW}(H_\delta) > 5.0 \text{ \AA}$ as the selection criterion for blue HDS.

On the contrary, normal early-type galaxies in the red half of the plane generally show little or no signs of star formation, and can be reproduced by a model with an exponentially decaying SFR with time scale $\tau = 1.0$ Gyr. The model iv) with solar metallicity (see the notes above) has $\text{EW}(H_\delta) < 3.0 \text{ \AA}$ when $D_n(4000) > 1.45$. Therefore, for red HDS galaxies we adopted a threshold of 3 \AA . Note that these selection criteria are equivalent to those adopted by Balogh et al. (1999), derived by using PEGASE models. None of the GISSEL03 models used here describes well red HDS galaxies and require the introduction of other ingredients, as discussed in Sect. 6.

⁴ Note that models with $Z=0.4Z_\odot$ and $Z=2.5Z_\odot$ would lead to the same result (see left and right panel in Fig. 3).

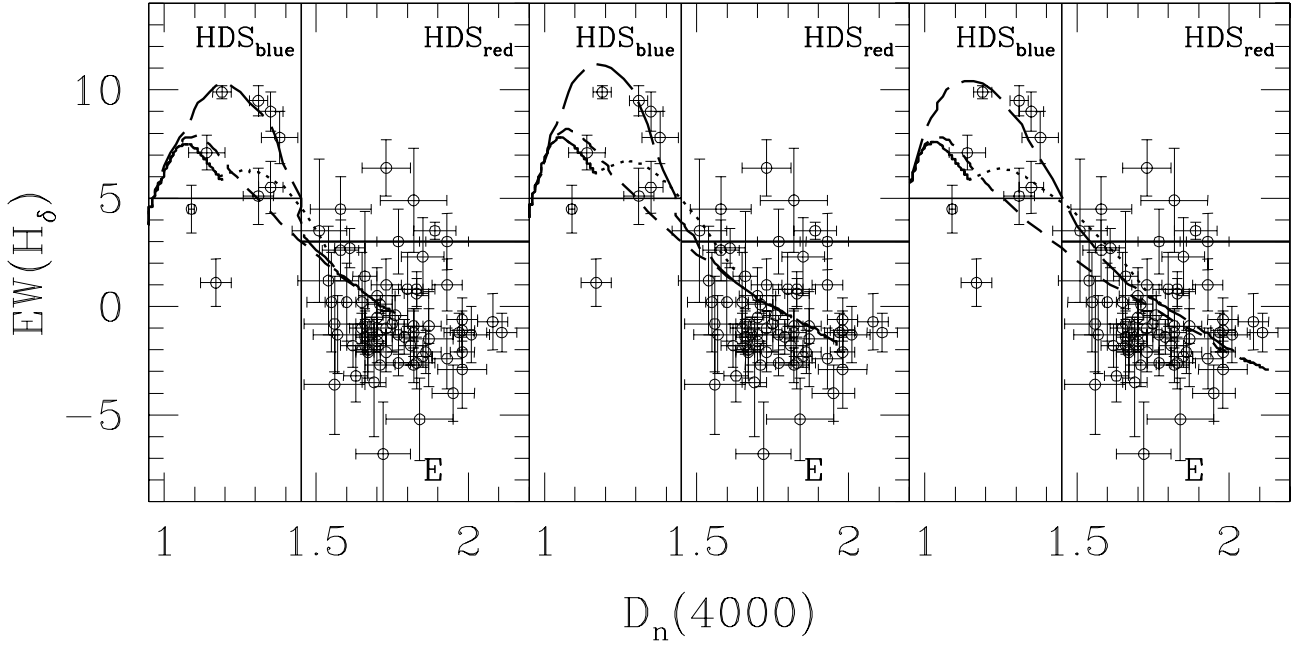


Fig. 3. Equivalent width of H_{δ} in \AA versus $D_n(4000)$ for 76 member galaxies compared to different GISSEL03 models. Left panel shows models with $Z=0.4Z_{\odot}$, while the central and right panels refer to Z_{\odot} and $2.5Z_{\odot}$, respectively. In each panel, the short dashed curves represent a model with exponential declining SFR with $\tau=1.0$ Gyr, while for the continuous and dotted lines the decay parameter is $\mu=0.01$. For the last one, the star formation is truncated at $t=10$ Gyr. The long dashed lines represent a model with an initial 100 Myr burst.

5% of cluster galaxies are classified as blue HDS galaxies and 7% as red HDS galaxies.

4.4. Passive galaxies

We define as passive, galaxies with no detectable emission lines and $EW(H_{\delta}) < 3.0 \text{\AA}$. These criteria are chosen to select galaxies without significant star formation, whose star formation history can be modeled by the exponentially decaying rate with $\tau = 1.0$ Gyr. Selected passive galaxies are mostly morphologically ellipticals or S0s as is shown below.

81% of member galaxies are classified as P galaxies.

5. Comparison with structural properties

We analysed the spectral properties of disk and spheroidal galaxies, separately (see La Barbera et al. 2003). We define as spheroids the objects with the Sersic index $n > 2$, and the remaining as disks. This corresponds to distinguishing between galaxies with a low bulge fraction ($< 20\%$) and those with a more prominent bulge component (van Dokkum et al. 1998).

In Fig. 4 the Sersic index is plotted against the B-R colour corrected for the effect of the CM relation, and different symbols are used to distinguish the different galaxy spectral types. This plot shows that there is a marked correspondence between spectral and structural properties: blue disks are ELG or HDS_{blue} galaxies while red spheroids are P or HDS_{red} galaxies. The converse is also true with some exceptions. Noticeably, one HDS_{blue} and two ELG galaxies have $2 < n < 4$, and one P galaxy has blue colour. By a visual inspection of R-band images, the two ELGs show signs of spiral arms (Fig. 5 left and central panels). We note that one of those is also close to the P galaxy with blue colour (see Fig. 4 and Fig. 5 left panel). Since the HDS_{blue} galaxy is close to a bright star (Fig. 5 right panel), its morphological classification could be wrong.

For the eight red P galaxies having Sersic index less than 2 we suggest that they are a population of disk galaxies. van den Berg, Pierce & Tully (1990), classifying 182 galaxies in the Virgo cluster, have shown the existence of “anemic” spiral galaxies, i.e. spiral galaxies deficient in neutral hydrogen. They have shown that these observations may be accounted for by assuming that gas has been stripped from the outer parts of these objects. Following van den Berg 1991 we recognize these galaxies as Ab-spirals and treat them as a different sample of galaxies from that of ellipticals.

HDS_{red} galaxies have all Sersic indices greater than 3, so they seem to be early-type galaxies.

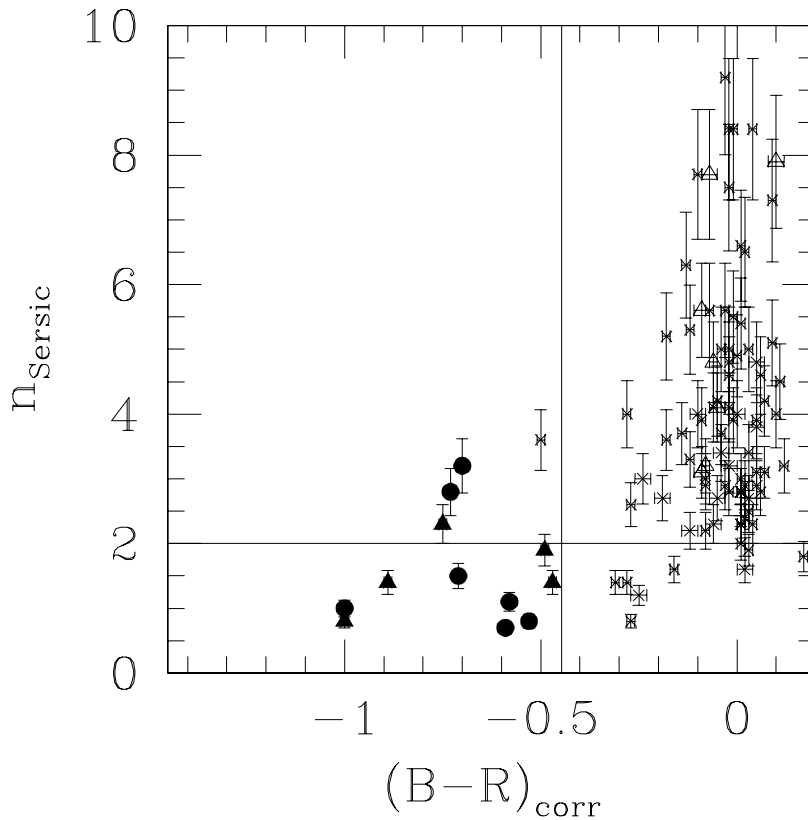


Fig. 4. Comparison between B–R galaxy colours and Sersic indices (n_{Sersic}). The vertical line marks the separation between blue and red galaxies (see text), while the horizontal line is the separation between disks and spheroids. Filled circles and triangles indicates ELG and HDS blue galaxies, respectively, while crosses and open triangles are for P and HDS red galaxies.

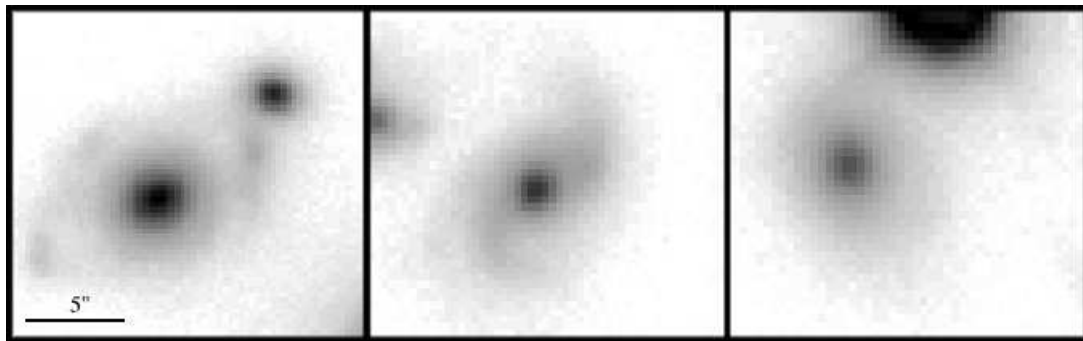


Fig. 5. R–band image of the four galaxies discussed in the text, with North at top and East to left. Scale is indicated in the left panel.

6. Distribution of ages

In order to follow the evolution of galaxies belonging to different spectral classes, we compare the strengths of various spectral indices in the observed galaxy spectra to stellar population models with different star formation rates and metallicities.

Bruzual & Charlot (2003) defined those indices that are most suitable in their models to investigate galaxy populations. They suggested two sets of spectral indices that should be fitted simultaneously in order to break the age-metallicity degeneracy: one of them being primary sensitive to the star formation history ($D_n(4000)$, H_β , $H_{\gamma A}$ and $H_{\delta A}$) and the other primary sensitive to metallicity ($[MgFe]'$, $[Mg_1Fe]$ and $[Mg_2Fe]$). The latter indices, in fact, are sensitive to metallicity but do not depend sensitively on changes in alpha-element to iron abundance ratios (see Thomas et al. 2003 and Bruzual & Charlot 2003 for details).

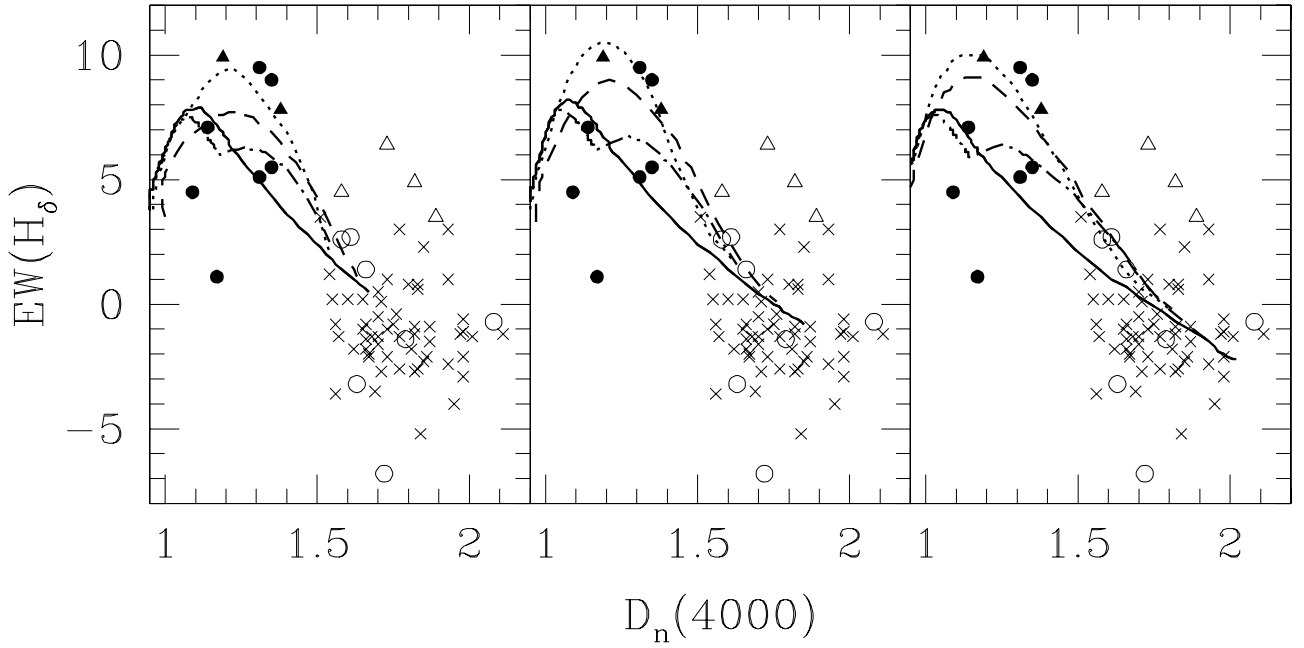


Fig. 6. Equivalent width of H_{δ} in \AA versus the break at 4000\AA for galaxies of different spectral types and GISSEL03 models. Filled and open circles, filled and open triangles, and crosses denote ELG, Ab-spiral, HDS_{blue} , HDS_{red} and P galaxies, respectively. The left panel shows models with $Z=0.4Z_{\odot}$, central and right panels $1Z_{\odot}$ and $2.5Z_{\odot}$, respectively. In each panel it is plotted a model with exponential declining SFR with time scale $\tau=1.0$ Gyr lasting 11 Gyr (continuous line), with superimposed a burst at $t=9$ Gyr, involving 10% (dashed line) or 40% (dotted line) of the total mass, and a model with continuous star formation truncated at $t=10$ Gyr (dot-dashed line). Note that models with continuous star formation stop at $D_n(4000)=1.2$ as it is better shown by the continuous line in Fig. 3.

For these reasons we use models with different star formation histories in order to fit simultaneously the observed strength of $D_n(4000)$, $H_{\delta A}$, $H_{\gamma A}$, H_{β} , $[\text{MgFe}]'$, $[\text{Mg}_1\text{Fe}]$, and $[\text{Mg}_2\text{Fe}]$.

We performed a chi-square minimization by using for each galaxy the available spectral indices. Uncertainties on ages were estimated performing Monte Carlo simulations. In each simulation, random shifts were added to the best-fit EWs according to the estimated errors on the spectral indices, and the uncertainty on age was obtained as the standard deviation of the age distribution.

P-galaxies (crosses in Fig. 6) exhibit moderate dispersion in $D_n(4000)$, caused by a combination of age and metallicity effects and little star formation. They are well described by an exponentially declining star formation with time scale $\tau=1.0$ Gyr (Merluzzi et al. 2003 and references therein). Assuming this SFR and metallicities $Z=0.4 Z_{\odot}, Z_{\odot}, 2.5 Z_{\odot}$, the distribution of ages for early-type galaxies, (Fig. 7), shows that the age of the bulk of ellipticals in ABCG 209 is greater than ~ 7 Gyr and that there is a tail toward younger ages up to ~ 4 Gyr. This translates into a formation epoch $z_f \gtrsim 1.6$ for the majority of ellipticals and $z_f \gtrsim 0.7$ for the younger population. The KMM algorithm (cf. Ashman et al. 1994 and refs. therein) suggests that a mixture of two Gaussians (with $n_1 = 19$, and $n_2 = 55$ members) is a better description of this age distribution (although only at $\sim 90\%$ c.l.). In this case, the mean ages of the two distributions are $t_1 = 5.8 \pm 0.8$ Gyr, and $t_2 = 9.2 \pm 1.2$ Gyr respectively. Thus, 74.3% of early-type galaxies seem to be coeval and to be formed early during the initial collapse of the cluster, at $z_f \gtrsim 3.5$. The remaining 25.7% is constituted by a younger galaxy population, that could be formed later ($z_f \gtrsim 1.2$) or could have experienced an enhancement in the star formation rate ~ 8.5 Gyr ago. This is in remarkable agreement with the trend with redshift of the total stellar mass in the cluster galaxies, derived from the colour-magnitude relation by Merluzzi et al. 2003 (see their Fig. 10).

As shown in Fig. 6 (filled circles), ELG galaxies can be fitted either by a model with truncated star formation history and by a model with a burst involving the 40% of the total mass (Fig. 6), whereas the two HDS_{blue} galaxies, for which we have the measurement of both $D_n(4000)$ and H_{δ} equivalent widths, seem to be reproduced only by a model with a short starburst. The starburst is assumed to begin at $t=9$ Gyr lasting for 0.1 Gyr. An equivalent width of H_{δ} greater than 5\AA implies that a starburst occurred in the galaxy before star formation was quenched, otherwise quiescent star formation activity would produce a spectrum with weaker Balmer lines (e.g., Couch & Sharples 1987; Poggianti & Barbaro 1996), as showed also by the comparison of the two models (dotted and dot-dashed lines) in Fig. 6. HDS_{blue} galaxies have EWs stronger than 5\AA , and thus could be post-starburst galaxies (but see below). The strength of the lines and the colour of these galaxies indicate an interruption of the star formation

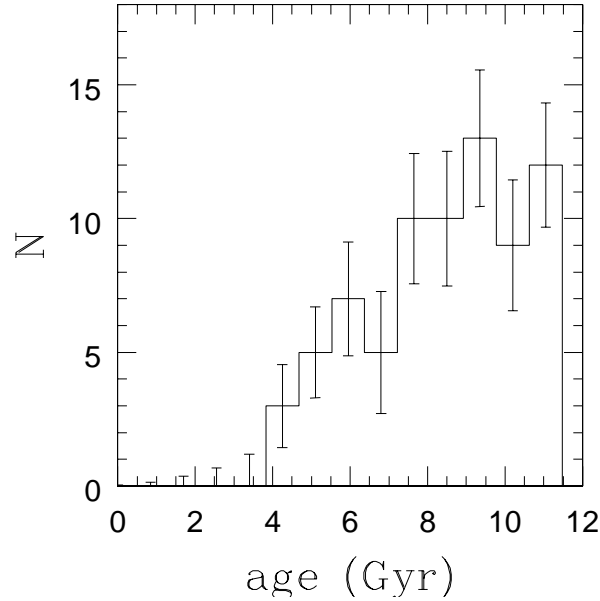


Fig. 7. Distribution of best-fitted ages of P galaxies (continuous line), by using a model with exponential declining SFR with time scale $\tau=1.0$ Gyr. Errors on ages are obtained performing 1000 simulations accounting for equivalent width measurement errors (see text)

within the last 0.5 Gyr, with a strong starburst preceding the quenching of star formation (see also Poggianti et al. 1999; Poggianti & Barbaro 1996).

In contrast, the typical time elapsed since the last star formation in the HDS_{red} will be in the range 1-2 Gyr, since this population exhibits weaker H_{δ} equivalent widths. However, the observed H_{δ} values for HDS_{red} tend to be larger than those predicted by both starburst and truncated star formation models, except from one galaxy that is well reproduced by a burst model (observed ~ 1 Gyr after the burst). This problem was pointed out by several authors (e.g. Couch & Sharples 1987, Morris et al. 1998, Poggianti & Barbaro 1996, Balogh et al. 1999) and will persist if photometric colours are considered instead of $D_n(4000)$. Models with IMFs biased toward massive stars are able to reproduce better these data. However, the stellar population resulting from such a burst is very short lived (~ 300 Myr), thus it is unlikely that many of these red galaxies are undergoing such bursts. Stronger H_{δ} equivalent widths may also be produced by temporal variations in the internal reddening in truncated or burst models. Balogh et al. (1999) have shown that by reddening the model it is possible to recover the observed data. This supports the idea that dust obscuration may play an important role in the appearance of these spectra. Recently, in fact, Shioya, Bekki & Couch (2004) demonstrates that the reddest HDS galaxies can only be explained by truncated or starburst models with very heavy dust extinction ($A_V > 0.5$ mag).

We run Bruzual & Charlot (2003) models with dust extinction, in order to check if the typical amount of dust content of galaxies can explain the red colour of HDS_{red} galaxies. We used the standard values of dust extinction: $\tau_V^{\text{BC}} = 1.0$ and $\tau_V^{\text{ISM}} = 0.5$ reported by Charlot & Fall (2000). As shown in Fig. 8, the typical amount of dust content in galaxies is inadequate to explain the colour of HDS_{red} galaxies.

7. Dynamical scenario

The analysis of the velocity distribution for all member galaxies of ABCG 209 (Mercurio et al. 2003a) shows the existence of a peak at $\langle z \rangle = 0.2090 \pm 0.0004$ with a line-of-sight velocity dispersion $\sigma_v = 1394^{+88}_{-99}$ km s $^{-1}$.

In order to check for possible variations of $\langle z \rangle$ and σ_v for different spectral types we analysed separately ELG, HDS_{blue} , Ab-spirals, HDS_{red} , and P galaxies. All galaxy populations show consistent mean redshift suggesting that they are really cluster populations and not merely foreground or background objects. On the other hand, the velocity dispersions of different classes show significant differences (see Table 3).

P galaxies define the mean redshift and the velocity dispersion of the cluster. The very low value of the velocity dispersion of HDS_{red} galaxies indicates that they could constitute a group of galaxies located at the cluster redshift. These post-starburst galaxies could be the remnant of the core of an infalling clump, that have suffered significant ram-pressure stripping in crossing the cluster core, preceded by an instantaneous burst of star formation.

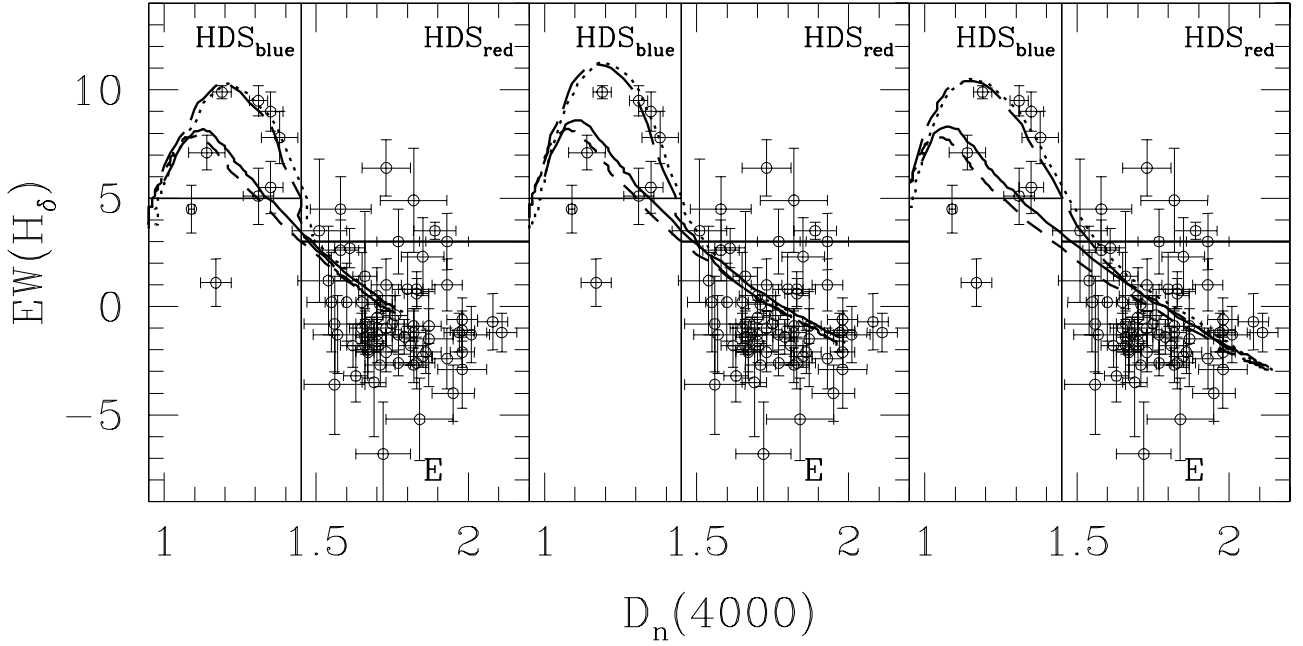


Fig. 8. Equivalent width of H_δ in \AA versus $D_n(4000)$ for 76 member galaxies compared to different GISEL03 models. Left panel shows models with $Z=0.4Z_\odot$, while the central and right panels refer to Z_\odot and $2.5Z_\odot$, respectively. In each panel, the short and the long dashed curves represent a model with exponential declining SFR with $\tau=1.0$ Gyr and with an initial 100 Myr burst without dust respectively. The continuous and the dotted lines draw the same models with dust extinction with $\tau_V^{\text{BC}} = 1.0$ and $\tau_V^{\text{ISM}} = 0.5$.

Table 3. Redshifts and velocity dispersion of different spectral classes. The biweight estimators (Beers et al. 1990) were used to derive the values

Class	N_{gal}	Redshift	σ_v
ALL	112	0.2090 ± 0.0004	1394^{+88}_{-99}
P	74	0.2086 ± 0.0005	1323^{+127}_{-94}
HDS _{red}	7	0.2087 ± 0.0005	339^{+91}_{-46}
Ab – spirals	8	0.2107 ± 0.0017	1295^{+340}_{-102}
HDS _{blue}	5	0.2071 ± 0.0044	2257^{+1085}_{-65}
ELG	7	0.2070 ± 0.0038	2634^{+712}_{-53}

The groups of ELG and HDS_{blue} galaxies exhibit very high velocity dispersions. The high velocity dispersions of these populations of disk-dominated galaxies indicate that they do not constitute a single infalling bound group but that they are the result of the growing of the cluster through the accretion of field galaxies. They have very similar spectral, photometric and structural properties and only slight difference in the velocity dispersion. On the other hand, they lie in regions with different density (see below).

Figure 9 shows the spatial distribution of different spectral classes. Taking into account the SE-NW elongation of the cluster, ELGs (filled circles) seem to be uniformly distributed in the outer parts of the cluster, while blue HDS galaxies (filled triangles) show a preferential location within the cluster. They are concentrated around the centre of the cluster along a direction perpendicular to the cluster elongation. P galaxies (crosses) are uniformly distributed over the whole cluster plane and red HDS galaxies (open triangles) lie around the centre along the cluster elongation. Ab–spirals (open circles) avoid the highest density regions, in agreement with those found by Goto et al. (2003c).

By using the information about the phase-space distributions, it is possible to find segregations of the various galaxy populations. Biviano et al. (2002) searched for segregation by comparing (R, v) -distributions in the clusters of the ESO Nearby Abell Cluster Survey, using the combined evidence from projected positions and relative velocities (they may not be independent). They also stressed the importance of the estimate of the projected clustercentric distance R , in order to make the comparison as unbiased as possible.

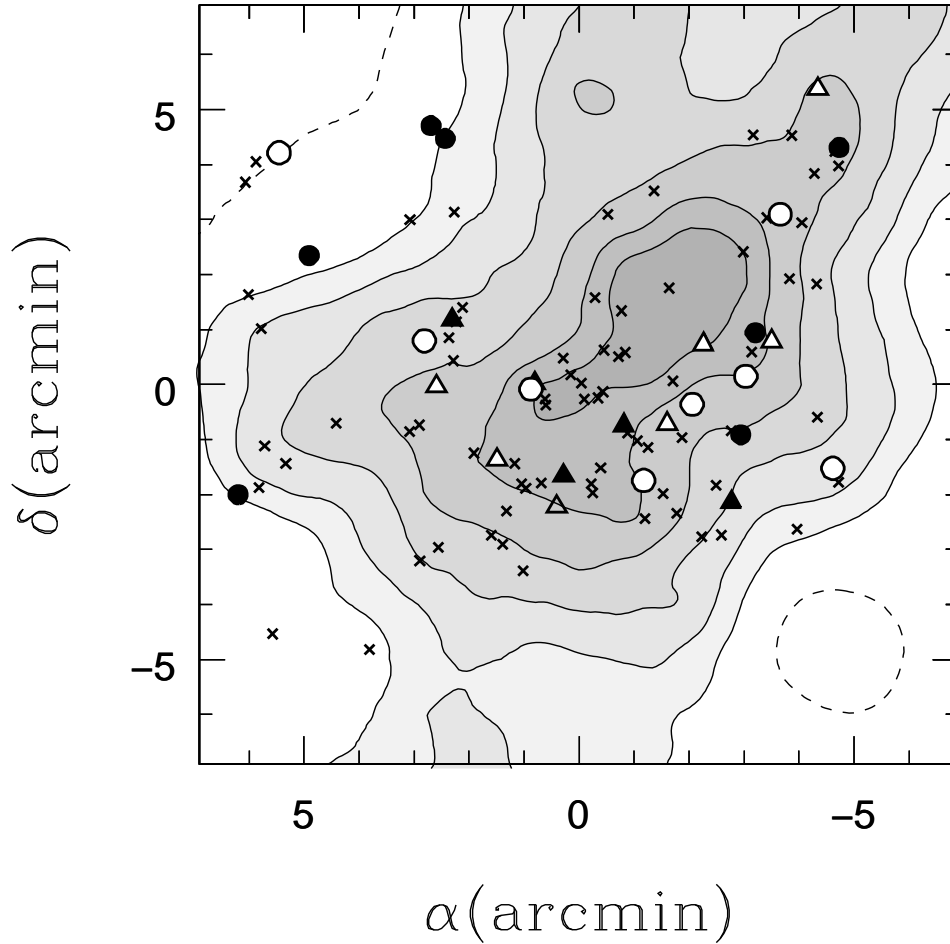


Fig. 9. Spatial distribution of different spectral classes. Filled and open circles, filled and open triangles, and crosses denote ELG, Ab-spiral, HDS_{blue}, HDS_{red} and P galaxies, respectively. The plot is centred on the cluster center. The dashed contour corresponds to the field galaxy number density, while the solid contours correspond respectively to the background subtracted 2, 3.3, 5, 7.5, 10, and 12.5 galaxies arcmin⁻²

The spatial distribution of galaxies in ABCG 209 shows a complex structure, characterised by an elongation in the SE-NW direction (see Mercurio et al. 2003a). To measure the effect of the cluster environment on the galaxy population, their spectral properties should be measured against the parameter most related to the cluster structure, which is the local galaxy number surface density rather than cluster-centric radius.

The local surface density (LD) of galaxies was determined across the CFHT images by Haines et al. (2004). We performed the comparison of (LD, v)-distributions by means the two-dimensional Kolmogorov-Smirnov test (hereafter 2DKS-test; Press et al. 1992). The 2DKS test is relatively conservative: if it indicates that two distributions have a high probability of not being drawn from the same parent population, other tests (e.g. Rank-Sum tests or Sign Tests) indicate the same thing, while the contrary is not always true. Moreover, the 2DKS test turns out to be reliable with relatively small samples (e.g. Biviano et al. 2002).

According to the 2DKS-test, we find significant evidence for segregation of ELGs with respect to both Ps (99.5%) and HDS_{blue} galaxies (97.6%), where ELGs lie in regions with lower density than P and HDS_{blue} galaxies. Moreover the distributions of HDS_{blue} and HDS_{red} galaxies differ at 90.7% c.l. and HDS_{blue} and Ab-spirals at 92.0%. These results show the effects of the cluster environment on the spectral properties of their constituents and support the scenario in which spirals are accreted into the cluster from the field, then star formation is stopped, the galaxies become gas-deficient, and eventually undergo a morphological transformation (Couch et al. 1998). This scenario may also account for the existence of anemic spirals (Ab-spirals in Table 3), whose velocity dispersion is fully consistent with those of the cluster.

8. Summary and Discussion

In order to investigate the nature of the galaxy population in ABCG 209, we have performed a detailed study of the photometric and spectroscopic properties of luminous member galaxies ($R \lesssim 20.0$). The primary goal of this analysis was to study the relation between cluster dynamics and evolution of stellar populations, and the effects of cluster environment on the properties of galaxies.

ABCG 209 is undergoing strong dynamical evolution with the merging of at least two clumps along the SE-NW direction, as indicated by i) the presence of a velocity gradient along a SE-NW axis, ii) the elongation of X-ray contour levels in Chandra images, and iii) the presence of substructures manifest both in the detection of two peaks separated by 50 arcsec in the X-ray flux and in the analysis of the velocity distribution, that showed three sub-clumps (Mercurio et al. 2003a). Moreover, the young dynamical state of the cluster is indicated by the possible presence of a radio halo (Giovannini, Tordi & Feretti 1999), which has been suggested to be the result of a recent cluster merger, through the acceleration of relativistic particles by the merger shocks (Feretti 2002).

The analysis of the spectroscopic and photometric properties of 102 cluster members has shown the presence of five different types of galaxies: i) passive evolving galaxies (P), which exhibit red colours and no emission lines, ii) emission line galaxies (ELG), which are blue and have prominent emission lines, iii) strong blue H_δ galaxies (HDS_{blue}), that are characterized by the presence of strong H_δ absorption lines ($EW(H_\delta) > 5 \text{ \AA}$) and blue colours, iv) strong red H_δ galaxies (HDS_{red}) galaxies, having $EW(H_\delta) > 3 \text{ \AA}$ and red colours; v) anemic spirals (Ab-spirals), that have the same spectral properties of passive evolving galaxies, but are disk-dominated systems.

P galaxies represent $\sim 74\%$ of the cluster population, and lie mainly in high density regions. Their age distribution is characterized by the presence of an “old population” formed early during the initial collapse of the cluster at ages greater than 7 Gyr, and another one, younger, that could be formed later or could have experienced an enhancement in the star formation rate.

ELGs lie in low density regions and have high line-of-sight velocity dispersion. Both the spatial position and the velocity dispersion suggest that this is a population of galaxies that has recently fallen into the cluster. This infall has induced a truncation of the star formation with, possibly, an associated short starburst. In fact, as shown in Fig. 6 (compare also with Fig. 3), only one ELG galaxy is consistent with continuous the star formation model before truncation.

These results are understandable in terms of cosmological models of structure formation, in which galaxies form earliest in the highest-density regions corresponding to the cores of rich clusters. Not only do the galaxies form earliest here, but the bulk of their star formation is complete by $z \sim 1$, at which point the cluster core is filled by shock-heated virialised gas which does not easily cool or collapse, suppressing the further formation of stars and galaxies (Blanton et al. 1999; 2000). Diaferio et al. (2001) shows that as mixing of the galaxy population is incomplete during cluster assembly, the positions of galaxies within the cluster are correlated with the epoch at which they were accreted. Hence galaxies in the cluster periphery are accreted later, and so have their star formation suppressed later, resulting in younger mean stellar populations. It should be considered however that this is a small-scale affect, and that this result in fact confirms that the red sequence galaxy population is remarkably homogeneous across all environments.

A similar scenario is suggested also by the velocity dispersion and the spectral properties of HDS_{blue} galaxies, which, however, are found to be aligned in a direction perpendicular to the cluster elongation, that coincides with the elongation of the X-ray contour levels in the Chandra images (see Fig. 14 in Mercurio et al. 2003a). As already pointed out by Poggianti et al. (2004) analysing the position of the strongest k+a galaxies (having $EW(H_\delta) > 5 \text{ \AA}$) in Coma, the correlation between the location of the post-starburst galaxies and the substructures in the intracluster medium strongly suggest that the truncation of the star formation activity in these galaxies, and possibly the previous starburst, could be the result of an interaction with the hot intracluster medium. Thus, the origin of HDS_{blue} could be a cluster related and, in particular, an ICM-related phenomenon, closely connected with the dynamical state of the cluster (see Poggianti et al. 2004). On the other hand, other possible explanations are reported in literature for the origin of HDS galaxies (e.g. Zabludoff et al. 1996, Balogh et al. 1999, Goto 2003d, Quintero et al. 2003). In particular, an open question is whether the burst is related to galaxy–galaxy or galaxy–cluster interactions.

HDS_{red} galaxies are distributed along the elongation of the cluster, mainly in intermediate density regions and have a low velocity dispersion. According to the evolution models, the presence of strong H_δ absorption line in their spectra indicates that these galaxies have experienced a short starburst of star formation in the past few Gyr. The measured $D_n(4000)$ of these galaxies can be made consistent with short starburst models only in presence of a substantial reddening by dust. In the starburst model, $EW(H_\delta)$ and $D_n(4000)$ decline on a timescale of ~ 2 Gyr after the burst has ceased, regardless of their SFR before the burst. This implies that, in the galaxies we observe, the burst has occurred no more than 4.5 Gyr ago.

As also indicated by the low value of the velocity dispersion, HDS_{red} galaxies could be the remnant of the core of an infalling clump of galaxies, that have experienced a merger with the main cluster. This merger may have induced a time–dependent tidal gravitational field that stimulated non–axisymmetric perturbations in the galaxies, driving effective transfer of gas to the central galactic region and, finally, triggering a secondary starburst in the central part of these galaxies (Bekki 1999). The second peak of the X-ray distribution could be related to the presence of this small galaxy group.

Considering that the mass is proportional to the cube of the measured velocity dispersion (see eq. (4) and (11) of Girardi et al. 1998), the ratio between the mass of the cluster as constituted only by P galaxies and the group of HDS_{red} galaxies is ~ 0.017 . Taffoni et al. (2003) studied the evolution of dark matter satellites orbiting inside more massive haloes, by using semi-analytical tools coupled with high-resolution N-body simulations. They explored the interplay between dynamic friction and tidal mass loss/evaporation in determining the final fate of the satellite, showing that, for satellites of intermediate mass ($0.01 M_h < M_{s,0} < 0.1 M_h$, where $M_{s,0}$ is the initial mass of the satellite and M_h is the mass of the main halo), the dynamical friction is strong and drives the satellite toward the centre of the main halo, with significant mass loss. The final fate depends on the concentration

of the satellite, relative to that of the main halo. Low-concentration satellites are disrupted, while high-concentration satellites survive, with a final mass that depends on the decay time.

Although both HDS_{blue} and HDS_{red} are characterized by the presence of strong Balmer lines, their colours and structural parameters show that they are two different galaxy populations. Deriving the Sersic index, we found that HDS_{blue} galaxies are disk-dominated galaxies while HDS_{red} are spheroids. On the contrary, Poggianti et al. (2004) found that, with the exception of two blue k+a galaxies compatible with a de Vaucouleurs' profile, all the other blue and red k+a galaxies in the Coma cluster have exponential or steeper profiles. This apparent contradiction may be overcome by considering the time for a HDS_{blue} galaxy to become red due to the damping of star formation is shorter than the difference in look-back time between ABCG 209 and Coma. It is thus conceivable that the HDS_{blue} galaxies we observe at $z \sim 0.21$ will turn into HDS_{red} galaxies observed Coma.

All the presented results support an evolutionary scenario in which ABCG 209 is characterized by the presence of two components: an old galaxy population, formed very early ($z_f \gtrsim 3.5$) and a younger population of infalling galaxies. Moreover, this cluster may have experienced, 3.5-4.5 Gyr ago, a merging with an infalling galaxy group. The merger of the cluster with the infalling group could have also powered the observed radio halo. In fact, merger activity and high ICM temperature may be responsible for producing a radio halo (Liang et al. 2000), because merging can provide enough energy to accelerate the electrons to relativistic energies, give rising to non-thermal emission. After the shock disappeared, radio halos may be maintained in situ by electron acceleration in the residual turbulence.

Appendix A

The equivalent width is defined by:

$$\text{EW} = \sum_{i=1}^N \frac{F_{Ci} - F_i}{F_{Ci}} \Delta\lambda, \quad (1)$$

where F_i is the flux in the pixel i , N is the number of pixels in the integration range, $\Delta\lambda$ is the dispersion in $\text{\AA}/\text{pixel}$ and F_{Ci} is the straight line fitted to the blue and the red pseudo-continuum intervals, evaluated in the pixel i (pixels with values more than 3σ away from the continuum level were rejected).

An index measured in magnitudes is:

$$\text{Mag} = -2.5 \log \left[1 - \frac{\text{EW}}{(\lambda_2 - \lambda_1)} \right], \quad (2)$$

where λ_1 and λ_2 are the wavelength limits of the feature bandpass.

The errors of the equivalent width measurement are estimated from the following relation (Czoske et al. 2001):

$$\sigma_{EW}^2 = \left(\frac{S}{N} \right)^{-2} \left[(N\Delta\lambda - \text{EW})\Delta\lambda + \frac{(N\Delta\lambda - \text{EW})^2}{N_1 + N_2} \right], \quad (3)$$

where S/N is the signal-to-noise ratio evaluated in the feature bandpass.

The local S/N for each galaxy is obtained by dividing the galaxy spectrum by its associated noise spectrum, as determined by adding in quadrature the Poisson noise (obtained through the IRAF task APALL) and the read-out noise of EMMI. The result is then fitted to remove residual features, and averaged over the wavelength range of the spectral feature to obtain the S/N ratio.

The catalogue of spectroscopic measurements is presented in Table 4.

Table 4. Spectroscopic data. Running number for galaxies in the presented sample (see also Table 1), ID (Col. 1); strength of the 4000 Å break (Col. 2); Cols. 3-15: equivalent widths. A value of '0.0' for the equivalent width for an emission-line indicates that no emission is observed, whereas '....' indicates that the equivalent width could not be measured as the line does not lie within the available wavelength range. The spectral classification adopted in the present paper is listed in the last column. ELG: emission line galaxies; HDS_{blue}: H_δ strong galaxies with blue colour; HDS_{red}: H_δ strong galaxies with red colour; P: passive evolving galaxies; Ab-spirals: passive evolving disk-dominated galaxies ($n_{\text{Sersic}} \leq 2$). Galaxy 62 presents very strong [OII], [OIII] and H_α emission, that could suggest the presence of an AGN. However, our data do not allow a reliable classification, leading us to exclude this object from the analysis.

ID	D _n (4000) Å	[OII] Å	H _δ Å Å	H _γ Å Å	Fe4531 Å	H _β Å	[OIII] Å	Fe5015 Å	Mg ₁ mag	Mg ₂ mag	Mgb Å	Fe5270 Å	Fe5335 Å	H _α Å	Spectral class
1	1.14 ± 0.06	-10.1 ± 1.2	7.1 ± 0.8	0.3 ± 0.8	4.7 ± 1.0	-0.5 ± 0.6	-0.3 ± 0.4	5.2 ± 1.2	0.07 ± 0.01	0.21 ± 0.02	3.4 ± 0.5	2.7 ± 0.6	2.0 ± 0.7	-10.8 ± 0.9	ELG
2	1.73 ± 0.03	0.0	-1.0 ± 0.8	-4.2 ± 0.7	4.3 ± 0.7	1.6 ± 0.5	0.0	6.1 ± 0.9	0.16 ± 0.01	0.30 ± 0.01	3.6 ± 0.4	3.6 ± 0.5	2.7 ± 0.6	2.5 ± 0.4	P
3	1.93 ± 0.05	0.0	1.0 ± 1.2	-2.8 ± 1.1	2.9 ± 1.1	2.5 ± 0.7	0.0	7.4 ± 1.3	0.15 ± 0.02	0.33 ± 0.02	5.6 ± 0.6	5.4 ± 0.7	2.2 ± 0.9	2.7 ± 0.6	P
4	-4.0 ± 2.2	1.4 ± 1.8	2.4 ± 2.1	4.2 ± 1.3	0.0	11.3 ± 2.5	0.12 ± 0.03	0.18 ± 0.04	3.9 ± 1.3	5.5 ± 1.4	3.4 ± 1.6	5.5 ± 1.2	P
5	1.72 ± 0.09	-6.8 ± 2.4	-1.8 ± 1.6	-0.4 ± 1.8	5.3 ± 1.0	0.0	5.4 ± 2.1	0.10 ± 0.02	0.27 ± 0.03	1.3 ± 1.0	5.9 ± 1.0	2.0 ± 1.3	-4.2 ± 1.1	Ab – spiral
6	1.89 ± 0.07	0.0	3.5 ± 0.4	-9.0 ± 0.5	2.6 ± 0.5	2.8 ± 0.3	0.0	10.6 ± 0.7	0.19 ± 0.01	0.44 ± 0.01	6.9 ± 0.3	6.4 ± 0.4	5.8 ± 0.5	3.6 ± 0.4	HDS _{red}
7	1.70 ± 0.03	0.0	-1.3 ± 0.7	-3.0 ± 0.6	4.1 ± 0.7	1.9 ± 0.4	0.0	5.1 ± 0.8	0.16 ± 0.01	0.34 ± 0.01	4.3 ± 0.4	3.1 ± 0.4	2.2 ± 0.5	0.3 ± 0.4	P
8	1.73 ± 0.05	0.0	1.0 ± 1.2	-3.9 ± 1.0	4.7 ± 1.0	1.3 ± 0.6	0.0	7.5 ± 1.2	0.19 ± 0.02	0.36 ± 0.02	5.2 ± 0.6	3.9 ± 0.7	2.3 ± 0.8	0.4 ± 0.6	P
9	-1.6 ± 1.6	-0.3 ± 1.3	4.8 ± 1.4	1.1 ± 0.9	0.0	6.0 ± 1.7	0.17 ± 0.02	0.34 ± 0.03	4.1 ± 0.8	4.4 ± 0.9	6.2 ± 1.0	0.4 ± 0.8	P
10	1.66 ± 0.06	-1.8 ± 1.7	-3.5 ± 1.4	4.2 ± 1.4	2.0 ± 1.0	0.0	7.0 ± 1.9	0.15 ± 0.02	0.31 ± 0.03	4.9 ± 0.8	3.1 ± 0.9	4.3 ± 1.1	4.6 ± 0.7	P
11	1.77 ± 0.04	0.0	-1.3 ± 0.9	-4.6 ± 0.8	4.4 ± 0.9	2.8 ± 0.5	0.0	5.4 ± 1.1	0.17 ± 0.01	0.32 ± 0.02	5.1 ± 0.5	3.1 ± 0.6	1.9 ± 0.6	1.8 ± 0.5	P
12	-2.7 ± 1.7	-8.4 ± 1.5	4.4 ± 1.6	4.0 ± 1.0	0.0	7.5 ± 2.0	0.24 ± 0.03	0.31 ± 0.03	4.0 ± 0.9	8.1 ± 1.0	2.8 ± 1.2	1.7 ± 1.0	P
13	2.8 ± 1.8	-2.8 ± 1.6	4.4 ± 1.7	1.0 ± 1.1	0.0	8.3 ± 2.0	0.14 ± 0.03	0.27 ± 0.03	2.8 ± 1.0	7.1 ± 1.0	4.7 ± 1.2	1.4 ± 0.9	P
14	2.08 ± 0.05	0.0	-0.7 ± 1.3	-2.8 ± 1.1	6.2 ± 1.2	3.2 ± 0.8	0.0	7.1 ± 1.6	0.17 ± 0.02	0.33 ± 0.02	4.2 ± 0.7	3.3 ± 0.8	1.9 ± 1.0	4.4 ± 0.6	Ab – spiral
15	3.9 ± 1.8	-2.1 ± 1.7	5.7 ± 2.0	5.8 ± 1.2	0.0	10.2 ± 2.3	0.11 ± 0.03	0.25 ± 0.04	3.8 ± 1.2	3.9 ± 1.3	6.0 ± 1.5	4.1 ± 1.2	HDS _{red}
16	1.80 ± 0.05	0.8 ± 1.7	-2.4 ± 1.4	5.8 ± 1.4	2.1 ± 0.9	0.0	5.9 ± 1.8	0.14 ± 0.02	0.27 ± 0.03	6.3 ± 0.8	3.3 ± 0.9	3.8 ± 1.1	1.7 ± 0.8	P
17	1.31 ± 0.03	9.5 ± 0.7	8.0 ± 0.7	3.0 ± 1.1	4.8 ± 0.6	-1.0 ± 0.5	3.6 ± 1.4	0.07 ± 0.02	0.15 ± 0.02	3.5 ± 0.7	4.0 ± 0.7	3.1 ± 0.9	-7.5 ± 0.9	ELG
18	-1.1 ± 1.7	-3.8 ± 1.5	5.8 ± 1.5	2.5 ± 1.0	0.0	9.0 ± 1.9	0.16 ± 0.02	0.34 ± 0.03	6.9 ± 0.9	4.5 ± 1.0	1.2 ± 1.3	2.5 ± 1.0	P
19	1.98 ± 0.05	-0.6 ± 1.0	1.5 ± 0.8	6.1 ± 0.8	2.4 ± 0.5	0.0	4.9 ± 1.0	0.15 ± 0.01	0.26 ± 0.01	5.0 ± 0.4	3.0 ± 0.5	7.4 ± 0.6	0.5 ± 0.4	P
20	1.66 ± 0.04	0.0	1.4 ± 3.0	-8.3 ± 2.7	4.5 ± 2.9	6.6 ± 1.7	0.0	7.2 ± 3.4	0.13 ± 0.04	0.30 ± 0.05	2.7 ± 1.7	2.7 ± 1.8	2.2 ± 2.1	1.7 ± 1.6	Ab – spiral
21	1.82 ± 0.04	0.0	-1.2 ± 1.1	-3.1 ± 0.9	4.9 ± 1.1	2.5 ± 0.7	0.0	7.5 ± 1.2	0.13 ± 0.02	0.29 ± 0.02	5.0 ± 0.6	3.4 ± 0.6	2.8 ± 0.8	3.4 ± 0.5	P
22	1.17 ± 0.05	4.6 ± 2.1	1.7 ± 1.0	8.7 ± 1.2	-3.0 ± 0.9	-2.5 ± 0.5	7.1 ± 1.5	0.04 ± 0.02	0.10 ± 0.02	4.7 ± 0.6	2.5 ± 0.8	7.2 ± 0.7	-5.6 ± 0.7	ELG
23	1.67 ± 0.04	0.0	-2.1 ± 0.9	-4.0 ± 0.8	4.9 ± 0.9	2.1 ± 0.6	0.0	6.0 ± 1.1	0.13 ± 0.01	0.26 ± 0.02	4.6 ± 0.5	4.9 ± 0.6	3.3 ± 0.7	2.7 ± 0.5	P

Table 4. Continued.

ID	$D_n(4000)$ Å	[OIII] Å	$H_{\delta A}$ Å	$H_{\gamma A}$ Å	Fe4531 Å	H_{β} Å	[OIII] Å	Fe5015 Å	Mg ₁ mag	Mg ₂ mag	Mgb Å	Fe5270 Å	Fe5335 Å	H_{α} Å	Spectral class
24	1.38 ± 0.06	7.8 ± 1.2	7.7 ± 1.1	4.0 ± 1.5	7.2 ± 0.8	0.0	7.4 ± 1.8	-0.02 ± 0.02	0.11 ± 0.03	3.8 ± 0.9	4.9 ± 1.1	-0.6 ± 1.5	0.7 ± 1.1	HDS _{blue}
25	1.84 ± 0.11	0.0	-5.2 ± 1.9	-5.5 ± 1.3	3.7 ± 1.3	5.3 ± 0.7	0.0	6.7 ± 1.4	0.15 ± 0.02	0.30 ± 0.02	4.8 ± 0.6	3.5 ± 0.7	3.3 ± 0.9	P
26	1.70 ± 0.03	-1.6 ± 1.0	-2.8 ± 0.8	5.2 ± 1.0	2.5 ± 0.6	0.0	6.0 ± 1.1	0.11 ± 0.01	0.27 ± 0.02	4.6 ± 0.6	2.5 ± 0.6	4.2 ± 0.7	2.9 ± 0.5	P
27	4.6 ± 2.2	-7.3 ± 2.2	11.8 ± 1.8	-0.3 ± 1.3	0.0	7.6 ± 2.5	0.18 ± 0.03	0.38 ± 0.04	7.6 ± 1.1	5.9 ± 1.3	4.9 ± 1.5	7.1 ± 1.0	HDS _{red}
28	1.67 ± 0.04	0.0	-2.0 ± 1.3	-2.8 ± 1.1	4.9 ± 1.1	5.1 ± 0.7	0.0	7.4 ± 1.4	0.13 ± 0.02	0.30 ± 0.02	4.8 ± 0.7	2.8 ± 0.7	2.8 ± 0.9	P
29	1.58 ± 0.06	0.0	2.6 ± 1.4	3.9 ± 1.1	5.6 ± 1.2	5.8 ± 0.7	0.0	5.4 ± 1.5	0.04 ± 0.02	0.16 ± 0.02	3.4 ± 0.7	4.9 ± 0.8	3.2 ± 0.9	3.6 ± 0.7	Ab – spiral
30	1.66 ± 0.03	0.0	-0.8 ± 0.6	-4.1 ± 0.5	4.3 ± 0.6	2.0 ± 0.4	0.0	5.2 ± 0.7	0.12 ± 0.01	0.29 ± 0.01	4.9 ± 0.3	3.1 ± 0.4	2.1 ± 0.5	-0.3 ± 0.4	P
31	1.87 ± 0.08	0.0	-1.5 ± 2.2	-1.5 ± 1.6	-1.9 ± 1.8	4.1 ± 0.9	0.0	6.9 ± 1.7	0.15 ± 0.02	0.30 ± 0.03	6.2 ± 0.8	5.5 ± 0.9	2.5 ± 1.0	1.2 ± 0.7	P
32	1.83 ± 0.04	0.0	0.6 ± 0.7	-4.5 ± 0.7	4.0 ± 0.7	3.0 ± 0.5	0.0	7.6 ± 0.9	0.15 ± 0.01	0.29 ± 0.01	4.2 ± 0.4	2.8 ± 0.5	1.2 ± 0.6	3.2 ± 0.4	P
33	1.83 ± 0.06	0.0	0.8 ± 0.8	-3.6 ± 0.8	3.4 ± 0.8	2.7 ± 0.5	0.0	5.6 ± 1.0	0.21 ± 0.01	0.39 ± 0.02	6.4 ± 0.5	3.5 ± 0.5	3.0 ± 0.6	2.3 ± 0.5	P
34	1.58 ± 0.10	0.0	4.5 ± 1.5	-3.7 ± 1.3	8.5 ± 1.3	4.9 ± 0.7	0.0	7.0 ± 1.5	0.09 ± 0.02	0.32 ± 0.02	6.4 ± 0.7	5.1 ± 0.8	0.9 ± 1.0	2.7 ± 0.6	HDS _{red}
35	1.73 ± 0.04	0.0	-2.1 ± 0.9	-3.5 ± 0.8	5.6 ± 0.8	3.6 ± 0.5	0.0	8.3 ± 1.0	0.13 ± 0.01	0.40 ± 0.02	7.1 ± 0.4	4.4 ± 0.5	4.7 ± 0.5	P
36	1.65 ± 0.06	0.2 ± 2.3	-3.5 ± 1.7	2.7 ± 1.9	2.5 ± 1.1	0.0	8.8 ± 2.1	0.14 ± 0.03	0.32 ± 0.03	4.9 ± 1.0	12.1 ± 1.0	3.8 ± 1.3	4.9 ± 0.9	P
37	1.97 ± 0.05	0.0	-1.2 ± 0.9	-5.1 ± 0.8	4.8 ± 0.7	1.4 ± 0.5	0.0	4.0 ± 1.0	0.18 ± 0.01	0.43 ± 0.02	6.5 ± 0.4	2.8 ± 0.5	2.4 ± 0.6	2.4 ± 0.5	P
38	1.95 ± 0.07	0.0	-4.0 ± 1.3	-3.3 ± 1.0	6.7 ± 0.9	3.2 ± 0.5	0.0	4.5 ± 1.0	0.21 ± 0.01	0.39 ± 0.02	6.3 ± 0.5	4.4 ± 0.5	2.9 ± 0.7	-0.4 ± 0.4	P
39	1.79 ± 0.04	0.0	-1.4 ± 0.8	-4.0 ± 0.7	4.7 ± 0.8	3.7 ± 0.5	0.0	7.1 ± 0.9	0.14 ± 0.01	0.36 ± 0.01	6.4 ± 0.4	3.5 ± 0.5	3.1 ± 0.6	2.3 ± 0.5	Ab – spiral
40	1.56 ± 0.10	-3.6 ± 2.3	1.8 ± 1.6	3.7 ± 1.9	2.0 ± 1.1	0.0	8.8 ± 2.1	0.04 ± 0.03	0.20 ± 0.03	4.1 ± 0.9	4.0 ± 1.1	5.3 ± 1.3	2.1 ± 0.9	P
41	1.85 ± 0.07	2.3 ± 1.8	-2.2 ± 1.4	9.0 ± 1.3	2.2 ± 0.9	0.0	10.4 ± 1.6	0.14 ± 0.02	0.29 ± 0.03	4.3 ± 0.7	2.4 ± 0.9	3.4 ± 1.0	4.3 ± 0.6	P
42	1.56 ± 0.10	-0.8 ± 2.2	3.9 ± 1.6	0.9 ± 2.0	3.6 ± 1.3	0.0	1.3 ± 2.6	0.12 ± 0.03	0.29 ± 0.04	5.6 ± 1.2	5.4 ± 1.2	2.3 ± 1.5	1.9 ± 1.1	P
43	1.19 ± 0.03	0.0	9.9 ± 0.3	6.7 ± 0.3	2.4 ± 0.5	7.7 ± 0.3	0.0	4.5 ± 0.6	0.04 ± 0.01	0.13 ± 0.01	1.7 ± 0.3	2.3 ± 0.4	2.5 ± 0.5	1.5 ± 0.4	HDS _{blue}
44	1.93 ± 0.05	0.0	-2.4 ± 1.4	-2.2 ± 1.1	4.9 ± 1.3	4.2 ± 0.7	0.0	7.1 ± 1.6	0.15 ± 0.02	0.38 ± 0.02	5.5 ± 0.7	3.5 ± 0.8	3.5 ± 0.9	-1.9 ± 0.8	P
45	1.98 ± 0.08	-2.9 ± 1.8	-3.7 ± 1.4	4.7 ± 1.5	3.6 ± 0.8	0.0	3.6 ± 1.7	0.22 ± 0.02	0.28 ± 0.02	7.2 ± 0.7	6.1 ± 0.8	4.2 ± 1.0	2.3 ± 0.8	P
46	1.83 ± 0.06	-2.6 ± 1.2	-4.7 ± 1.0	6.9 ± 1.1	3.2 ± 0.6	0.0	9.0 ± 1.2	0.24 ± 0.02	0.33 ± 0.02	1.5 ± 0.6	2.0 ± 0.7	3.0 ± 0.8	-1.4 ± 0.6	P
47	1.70 ± 0.04	0.0	-0.5 ± 0.8	-2.8 ± 0.7	5.6 ± 0.8	1.6 ± 0.5	0.0	6.1 ± 1.0	0.17 ± 0.01	0.35 ± 0.02	4.5 ± 0.5	3.9 ± 0.5	3.6 ± 0.6	3.4 ± 0.5	P
48	1.57 ± 0.08	0.0	-1.3 ± 1.8	-2.1 ± 1.5	4.1 ± 1.5	2.5 ± 0.9	0.0	9.4 ± 1.6	0.19 ± 0.02	0.29 ± 0.03	6.1 ± 0.8	2.1 ± 0.9	2.9 ± 1.0	3.4 ± 0.7	P
49	1.82 ± 0.03	-0.9 ± 0.7	-1.6 ± 0.6	6.0 ± 0.6	2.6 ± 0.4	0.0	6.0 ± 0.7	0.12 ± 0.01	0.30 ± 0.01	4.6 ± 0.3	3.2 ± 0.4	3.2 ± 0.5	P
50	-1.5 ± 0.7	-5.7 ± 0.6	4.0 ± 0.6	2.4 ± 0.4	0.0	5.8 ± 0.7	0.17 ± 0.01	0.35 ± 0.01	4.3 ± 0.3	3.6 ± 0.4	2.9 ± 0.4	3.7 ± 0.3	P

Table 4. Continued.

ID	$D_n(4000)$ Å	[OII] Å	$H_{\delta A}$ Å	$H_{\gamma A}$ Å	Fe4531 Å	H_{β} Å	[OIII] Å	Fe5015 Å	Mg ₁ mag	Mg ₂ mag	Mgb Å	Fe5270 Å	Fe5335 Å	H_{α} Å	Spectral class
51	1.65 ± 0.04	0.0	-1.0 ± 0.7	-1.1 ± 0.6	3.4 ± 0.7	3.6 ± 0.4	0.0	6.1 ± 0.8	0.12 ± 0.01	0.29 ± 0.01	4.3 ± 0.4	3.9 ± 0.5	2.9 ± 0.6	4.1 ± 0.4	P
52	1.81 ± 0.04	0.0	-1.8 ± 0.9	-3.3 ± 0.8	3.8 ± 0.8	2.4 ± 0.5	0.0	5.8 ± 1.0	0.17 ± 0.01	0.37 ± 0.02	5.7 ± 0.5	2.5 ± 0.5	2.8 ± 0.6	2.3 ± 0.5	P
53	1.51 ± 0.09	0.0	2.9 ± 3.3	-5.0 ± 2.3	4.5 ± 2.2	1.2 ± 1.2	0.0	5.4 ± 2.3	0.15 ± 0.03	0.34 ± 0.04	5.0 ± 1.0	2.1 ± 1.2	6.1 ± 1.3	4.1 ± 0.9	P
54	2.11 ± 0.05	0.0	-1.2 ± 0.9	-2.3 ± 0.8	4.1 ± 0.8	3.4 ± 0.5	0.0	7.8 ± 0.9	0.17 ± 0.01	0.39 ± 0.02	5.7 ± 0.5	4.3 ± 0.5	2.4 ± 0.7	2.3 ± 0.4	P
55	1.77 ± 0.04	0.0	-2.6 ± 0.6	-6.4 ± 0.6	4.9 ± 0.6	3.7 ± 0.4	0.0	5.0 ± 0.7	0.17 ± 0.01	0.41 ± 0.01	6.5 ± 0.3	2.2 ± 0.4	3.2 ± 0.5	1.4 ± 0.4	P
56	1.86 ± 0.05	0.0	-2.1 ± 1.0	-4.3 ± 0.8	2.6 ± 0.8	3.3 ± 0.5	0.0	4.9 ± 0.9	0.15 ± 0.01	0.38 ± 0.01	6.4 ± 0.4	2.9 ± 0.5	2.6 ± 0.6	0.7 ± 0.4	P
57	4.5 ± 1.3	0.3 ± 1.2	4.0 ± 1.4	1.5 ± 0.8	0.0	4.4 ± 1.6	0.08 ± 0.02	0.18 ± 0.02	3.2 ± 0.8	4.9 ± 0.8	3.3 ± 1.0	0.5 ± 0.7	HDS _{blue}
58	1.66 ± 0.03	0.0	-1.4 ± 0.8	-5.6 ± 0.7	5.0 ± 0.8	0.6 ± 0.5	0.0	5.5 ± 1.0	0.17 ± 0.01	0.39 ± 0.02	4.6 ± 0.5	3.4 ± 0.5	3.3 ± 0.7	2.5 ± 0.5	P
59	1.73 ± 0.08	0.0	6.4 ± 1.3	-2.9 ± 1.1	6.4 ± 1.1	-0.4 ± 0.7	0.0	8.9 ± 1.1	0.14 ± 0.01	0.29 ± 0.02	5.9 ± 0.6	3.7 ± 0.6	2.3 ± 0.8	1.9 ± 0.5	HDS _{red}
60	1.70 ± 0.06	0.0	0.5 ± 1.3	-3.3 ± 1.0	4.8 ± 1.0	3.0 ± 0.6	0.0	6.1 ± 1.2	0.15 ± 0.01	0.39 ± 0.02	7.5 ± 0.5	4.3 ± 0.6	4.0 ± 0.7	1.9 ± 0.5	P
61	1.69 ± 0.04	0.0	-3.5 ± 2.5	-2.5 ± 2.1	4.8 ± 2.4	2.3 ± 1.5	0.0	7.7 ± 2.7	0.19 ± 0.04	0.34 ± 0.05	5.5 ± 1.3	2.6 ± 1.6	4.4 ± 1.7	2.0 ± 1.2	P
62	1.09 ± 0.01	-57.6 ± 1.8	4.5 ± 1.1	-3.4 ± 1.2	6.5 ± 1.3	-19.1 ± 1.2	-22.9 ± 0.8	-11.4 ± 1.9	0.06 ± 0.02	0.05 ± 0.02	0.7 ± 0.9	1.2 ± 1.0	0.7 ± 1.1	-123.3 ± 1.6	?
63	-2.2 ± 1.1	-3.2 ± 1.0	4.4 ± 0.9	2.5 ± 0.5	0.0	5.1 ± 1.1	0.16 ± 0.01	0.37 ± 0.02	5.1 ± 0.5	4.2 ± 0.6	2.8 ± 0.7	1.3 ± 0.5	P
64	3.2 ± 1.3	-0.1 ± 1.3	4.4 ± 1.5	0.6 ± 1.1	0.0	4.8 ± 1.9	0.08 ± 0.02	0.20 ± 0.03	2.8 ± 0.9	4.6 ± 1.0	2.4 ± 1.3	-10.6 ± 1.1	HDS _{blue}
65	1.63 ± 0.04	0.0	-3.2 ± 1.2	-3.5 ± 1.0	6.3 ± 1.1	3.3 ± 0.7	0.0	7.8 ± 1.4	0.15 ± 0.02	0.21 ± 0.02	6.9 ± 0.7	4.5 ± 0.8	0.8 ± 0.9	-1.0 ± 0.8	Ab - spiral
66	-1.0 ± 1.6	-2.1 ± 1.3	4.4 ± 1.2	1.8 ± 0.8	0.0	7.0 ± 1.5	0.15 ± 0.02	0.32 ± 0.02	5.3 ± 0.6	3.6 ± 0.8	3.1 ± 0.9	2.1 ± 0.6	P
67	1.54 ± 0.10	1.2 ± 2.5	4.4 ± 1.7	10.5 ± 1.7	4.5 ± 1.1	0.0	-0.7 ± 2.2	0.17 ± 0.03	0.34 ± 0.03	2.9 ± 1.0	2.7 ± 1.1	2.1 ± 1.3	P
68	1.85 ± 0.03	0.0	-2.3 ± 0.5	-4.3 ± 0.5	4.6 ± 0.5	4.2 ± 0.3	0.0	6.5 ± 0.6	0.17 ± 0.01	0.38 ± 0.01	5.8 ± 0.3	3.5 ± 0.3	3.1 ± 0.4	1.5 ± 0.3	P
69	2.01 ± 0.06	0.0	-1.3 ± 1.3	-5.8 ± 1.1	4.3 ± 1.0	1.4 ± 0.7	0.0	6.5 ± 1.2	0.17 ± 0.01	0.40 ± 0.02	7.7 ± 0.5	4.5 ± 0.6	2.3 ± 0.7	2.5 ± 0.5	P
70	1.2 ± 1.7	-3.1 ± 1.4	2.9 ± 1.4	0.0	0.0	5.1 ± 1.7	0.13 ± 0.02	0.23 ± 0.02	3.8 ± 0.7	2.5 ± 0.8	3.7 ± 1.0	1.7 ± 0.5	P
71	1.98 ± 0.04	0.0	-1.1 ± 0.9	-3.0 ± 0.7	4.6 ± 0.8	3.3 ± 0.5	0.0	5.2 ± 0.9	0.18 ± 0.01	0.36 ± 0.02	5.1 ± 0.4	3.9 ± 0.5	2.2 ± 0.6	P
72	1.82 ± 0.11	4.9 ± 2.4	-11.1 ± 2.2	4.4 ± 2.0	5.1 ± 1.2	0.0	2.4 ± 2.3	0.20 ± 0.03	0.22 ± 0.03	5.5 ± 1.0	6.0 ± 1.1	4.3 ± 1.3	3.6 ± 0.9	HDS _{red}
73	1.87 ± 0.04	0.0	-0.9 ± 0.8	-3.7 ± 0.6	4.2 ± 0.7	3.7 ± 0.4	0.0	8.4 ± 0.9	0.16 ± 0.01	0.39 ± 0.01	6.1 ± 0.4	3.9 ± 0.4	3.3 ± 0.6	P
74	1.71 ± 0.04	0.0	0.1 ± 0.4	-3.6 ± 0.4	4.3 ± 0.5	2.6 ± 0.3	0.0	4.8 ± 0.7	0.14 ± 0.01	0.22 ± 0.01	2.3 ± 0.3	4.9 ± 0.4	3.2 ± 0.5	4.3 ± 0.3	P
75	1.93 ± 0.07	0.0	3.0 ± 1.3	-5.6 ± 1.4	2.0 ± 1.6	3.3 ± 1.3	0.0	2.6 ± 2.7	0.25 ± 0.04	0.79 ± 0.05	16.7 ± 1.0	-1.7 ± 1.6	0.6 ± 2.0	P
76	1.62 ± 0.04	0.0	-1.8 ± 1.0	-4.0 ± 0.9	2.7 ± 1.1	6.0 ± 0.7	0.0	3.1 ± 1.5	0.23 ± 0.02	0.42 ± 0.02	4.4 ± 0.7	3.1 ± 0.8	5.2 ± 0.9	P
77	1.71 ± 0.05	0.0	-2.7 ± 1.0	-6.1 ± 0.9	5.1 ± 1.0	1.9 ± 0.7	0.0	5.5 ± 1.4	0.20 ± 0.02	0.42 ± 0.02	5.6 ± 0.7	1.4 ± 0.8	2.5 ± 1.0	P

Table 4. Continued.

ID	$D_n(4000)$	[OII] Å	$H_{\delta A}$ Å	$H_{\gamma A}$ Å	Fe4531 Å	H_{β} Å	[OIII] Å	Fe5015 Å	Mg ₁ Å	Mg ₂ mag	Mgb mag	Fe5270 Å	Fe5335 Å	H_{α} Å	Spectral class
78	2.3 ± 2.9	0.5 ± 3.1	3.8 ± 3.5	4.5 ± 2.2	0.0	14.5 ± 5.9	0.02 ± 0.08	0.15 ± 0.10	4.8 ± 3.3	11.0 ± 3.2	-6.9 ± 6.1	P
79	5.1 ± 0.6	5.0 ± 0.5	3.1 ± 0.7	4.5 ± 0.4	0.0	6.6 ± 0.8	0.08 ± 0.01	0.19 ± 0.01	3.2 ± 0.4	3.8 ± 0.5	3.9 ± 0.6	2.5 ± 0.5	HDS _{blue}
80	0.3 ± 1.6	-4.7 ± 1.6	5.2 ± 1.8	4.4 ± 1.1	0.0	12.1 ± 2.2	0.10 ± 0.03	0.38 ± 0.04	6.1 ± 1.1	0.6 ± 1.4	5.2 ± 1.4	-3.6 ± 1.4	P
81	1.31 ± 0.05	-6.1 ± 1.7	5.1 ± 1.3	3.5 ± 1.3	4.8 ± 1.6	1.6 ± 1.1	-0.2 ± 0.8	0.5 ± 2.3	0.07 ± 0.03	0.23 ± 0.04	0.9 ± 1.2	6.0 ± 1.1	3.0 ± 1.4	-4.1 ± 1.3	ELG
82	-2.5 ± 1.3	-4.7 ± 1.1	4.6 ± 1.0	2.9 ± 0.6	0.0	7.6 ± 1.2	0.14 ± 0.02	0.35 ± 0.02	5.5 ± 0.6	3.1 ± 0.6	2.6 ± 0.7	2.2 ± 0.5	P
83	3.3 ± 1.6	-3.9 ± 1.7	-1.9 ± 2.3	2.9 ± 1.5	0.0	5.4 ± 3.6	0.05 ± 0.05	0.61 ± 0.07	11.8 ± 1.5	-11.8 ± 2.5	5.1 ± 2.5	HDS _{red}
84	1.35 ± 0.04	-6.5 ± 1.4	9.0 ± 0.9	2.4 ± 0.9	0.7 ± 1.3	3.7 ± 0.9	-1.1 ± 0.7	9.3 ± 1.8	0.02 ± 0.02	0.19 ± 0.03	3.9 ± 0.9	0.0 ± 1.1	2.1 ± 1.3	-6.0 ± 1.5	ELG
85	1.77 ± 0.07	0.0	3.0 ± 1.5	0.3 ± 1.5	0.5 ± 1.9	7.1 ± 1.2	0.0	10.7 ± 2.6	0.18 ± 0.04	0.52 ± 0.05	7.2 ± 1.3	0.8 ± 1.6	5.5 ± 1.9	-4.1 ± 2.8	P
86	1.98 ± 0.04	-2.1 ± 0.7	-4.0 ± 0.6	3.8 ± 0.6	2.1 ± 0.4	0.0	5.5 ± 0.7	0.16 ± 0.01	0.35 ± 0.01	4.5 ± 0.3	3.2 ± 0.4	2.4 ± 0.5	1.3 ± 0.3	P
87	1.68 ± 0.05	0.0	-1.3 ± 0.8	-3.1 ± 0.7	2.7 ± 0.8	2.2 ± 0.5	0.0	10.5 ± 0.9	0.20 ± 0.01	0.33 ± 0.01	4.7 ± 0.5	3.5 ± 0.5	0.6 ± 0.6	0.0 ± 0.5	P
88	1.60 ± 0.07	0.0	0.2 ± 1.8	-5.4 ± 1.7	5.0 ± 1.9	-0.4 ± 1.4	0.0	1.6 ± 2.8	0.04 ± 0.03	0.17 ± 0.04	2.2 ± 1.5	6.4 ± 1.5	4.6 ± 1.9	6.3 ± 2.0	P
89	1.75 ± 0.05	0.0	-0.8 ± 1.3	-1.6 ± 1.2	4.8 ± 1.4	4.3 ± 0.8	0.0	6.5 ± 1.6	0.19 ± 0.02	0.31 ± 0.03	4.4 ± 0.8	4.5 ± 0.9	1.9 ± 1.1	0.6 ± 0.9	P
90	1.7 ± 3.1	-3.5 ± 2.5	4.8 ± 2.3	3.7 ± 1.4	0.0	4.7 ± 2.6	0.11 ± 0.03	0.25 ± 0.04	5.2 ± 1.1	2.9 ± 1.3	3.2 ± 1.5	2.3 ± 0.8	P
91	-4.1 ± 1.1	-4.7 ± 1.0	4.1 ± 1.0	2.9 ± 0.6	0.0	5.1 ± 1.2	0.14 ± 0.01	0.37 ± 0.02	6.3 ± 0.5	4.0 ± 0.6	3.8 ± 0.8	1.9 ± 0.6	P
92	1.35 ± 0.04	-7.8 ± 1.9	5.5 ± 1.2	4.9 ± 1.2	3.4 ± 1.5	0.9 ± 1.0	-0.2 ± 0.7	3.8 ± 2.1	0.10 ± 0.03	0.22 ± 0.03	2.7 ± 1.1	2.8 ± 1.2	5.2 ± 1.3	-16.2 ± 1.8	ELG
93	-1.8 ± 0.7	-6.2 ± 0.6	5.0 ± 0.7	-0.1 ± 0.4	0.0	4.5 ± 0.8	0.20 ± 0.01	0.38 ± 0.01	5.2 ± 0.4	3.4 ± 0.4	3.1 ± 0.5	2.3 ± 0.3	P
94	1.61 ± 0.05	2.7 ± 0.9	-0.8 ± 0.9	5.5 ± 1.0	4.5 ± 0.6	0.0	7.7 ± 1.2	0.11 ± 0.02	0.36 ± 0.02	5.2 ± 0.6	0.9 ± 0.7	1.6 ± 0.9	-0.4 ± 0.8	Ab – spiral
95	-1.0 ± 0.9	-3.8 ± 0.8	4.7 ± 0.8	3.2 ± 0.5	0.0	9.6 ± 0.9	0.19 ± 0.01	0.37 ± 0.01	6.0 ± 0.4	4.3 ± 0.5	4.0 ± 0.6	0.8 ± 0.4	P
96	-1.5 ± 0.9	-4.6 ± 0.8	3.5 ± 0.9	4.6 ± 0.6	0.0	3.9 ± 1.2	0.16 ± 0.02	0.38 ± 0.02	6.3 ± 0.6	3.1 ± 0.7	3.3 ± 0.8	1.4 ± 0.7	P
97	1.55 ± 0.08	0.2 ± 2.3	-3.0 ± 2.2	3.3 ± 2.4	2.5 ± 1.5	0.0	13.2 ± 2.6	0.18 ± 0.04	0.26 ± 0.04	4.5 ± 1.4	11.7 ± 1.3	10.4 ± 1.4	4.9 ± 0.8	P
98	1.82 ± 0.05	-2.7 ± 0.8	-6.8 ± 1.4	4.4 ± 1.4	2.2 ± 0.8	0.0	10.2 ± 1.7	0.16 ± 0.02	0.31 ± 0.03	1.5 ± 1.0	5.7 ± 1.1	3.0 ± 1.3	-4.0 ± 1.9	P
99	1.76 ± 0.04	-0.4 ± 0.9	-6.6 ± 0.8	3.8 ± 0.8	3.7 ± 0.5	0.0	4.4 ± 1.0	0.11 ± 0.01	0.30 ± 0.02	4.2 ± 0.5	3.6 ± 0.5	3.2 ± 0.6	2.5 ± 0.5	P
100	3.0 ± 1.6	-10.1 ± 1.8	-0.9 ± 2.2	10.0 ± 1.4	0.0	9.5 ± 3.8	0.02 ± 0.04	0.21 ± 0.05	0.9 ± 1.8	6.4 ± 1.8	3.0 ± 2.2	-3.4 ± 1.8	Ab – spirals
101	0.3 ± 2.6	-4.4 ± 2.1	3.4 ± 2.1	6.7 ± 1.2	0.0	14.6 ± 2.6	0.18 ± 0.04	0.34 ± 0.05	10.2 ± 1.2	6.4 ± 1.4	-3.3 ± 2.2	1.8 ± 1.6	P
102	4.5 ± 1.0	-1.0 ± 1.0	4.0 ± 1.3	1.8 ± 0.9	-1.6 ± 0.7	8.8 ± 1.9	0.03 ± 0.02	0.11 ± 0.03	3.6 ± 1.0	-0.6 ± 1.2	2.3 ± 1.3	-6.9 ± 1.3	ELG

Acknowledgements. We are grateful to the referee, T. Goto, for his very accurate work on the paper. We are grateful to Stephan Charlot and Gustavo Bruzual who provided us with the galaxy models. We thank Andrea Biviano for useful discussions. A. M. thanks Massimo Capaccioli for useful discussions and for the hospitality at the INAF-Osservatorio Astronomico di Capodimonte, and Francesca Matteucci for support during this work.

References

- Abell, G. O., Corwin, H. G. Jr., & Olowin, R. P. 1989, *ApJs*, 70, 1
- Abraham, R.G., Smecker-Hane, T. A., Hutchings, J. B., et al. 1996, *ApJ*, 471, 694
- Ashman, K. M., Bird, C. M., & Zepf, S. E. 1994, *AJ*, 108, 2348
- Balogh, M. L., Morris, S.L., Yee, H.K.C., Carlberg, R.G., & Ellingson, E. 1999, *ApJ*, 527, 54
- Barger, A. J., Aragon-Salamanca, A., Ellis, R. S., et al. 1996, *MNRAS*, 279, 1
- Beers, T.C., Flynn, K., & Gebhardt, K. 1990, *AJ*, 100, 32
- Bekki, K. 1999, *ApJ*, 510, L15
- Biviano, A., Katgert, P., Thomas, T., & Adami, C. 2002, *A&A*, 387, 8
- Blanton, M., Cen, R., Ostriker, J. P., & Strauss, M. A. 1999, *ApJ*, 522, 590
- Blanton, M., Cen, R., Ostriker, J. P., Strauss, M. A., & Tegmark, M. 2000, *ApJ*, 531, 1
- Bruzual, G. 1983, *ApJ*, 273, 105
- Bruzual, G. & Charlot, S. 1993, *ApJ*, 405, 538
- Bruzual, G. & Charlot, S. 2003, *MNRAS*, 344, 1000
- Butcher, H. & Oemler, A. 1978, *ApJ*, 219, 18
- Butcher, H. & Oemler, A. 1984, *ApJ*, 285, 426
- Caldwell, N., Rose, J., Sharples, R. M., Ellis, R. S., & Bower, R. G. 1993, *AJ*, 106, 473
- Caldwell, N., & Rose, J. 1997, *AJ*, 113, 492
- Charlot, S. & Fall, S. M. 2000, *ApJ*, 539, 718
- Couch, W. J., & Sharples, R. M. 1987, *MNRAS*, 229, 423
- Couch, W. J., Ellis, R. S., Sharples, R. M., & Smail, I. 1994, *ApJ*, 430, 121
- Couch, W. J., Barger, A. J., Smail, I., Ellis, R. S. & Sharples, R. M. 1998, *ApJ*, 497, 188
- Czoske, O., Kneib, J. P., Soucail, G., et al. 2001, *A&A*, 372, 391
- Diaferio, A., Kauffmann G., Balogh, M. L., et al. 2001, *MNRAS*, 323, 999
- Dressler, A., & Gunn, J. E. 1982, *ApJ*, 263, 533
- Dressler, A., & Gunn, J. E. 1983, *ApJ*, 270, 7
- Dressler, A., & Gunn, J. E. 1992, *ApJS*, 78, 1
- Dressler, A., Oemler, A. J., & Couch, W. J. 1997, *ApJ*, 490, 577
- Ebeling, H., Voges, W., Böhringer, H., et al. 1996, *MNRAS*, 281, 799
- Ellingson, E., Lin, H., Yee, H. K. C., & Carlberg, R. G. 2001, *ApJ*, 547, 609
- Feretti, L. 2002, in ‘The Universe at Low Radio Frequences, eds A. Pramesh Rao, G. Swarup, & Gopal–Krishna (Kluwer Academic Publishers), S–199, (astro-ph/0006379)
- Giovannini, G., Tordi, M., & Feretti, L. 1999, *New Astronomy*, 4, 141
- Girardi, M., Giuricin, G., Mardirossian, F., Mezzetti, M., & Boschini, W. 1998, *ApJ*, 505, 74
- Goto, T., Yamauchi, C., Yataka, F., et al. 2003a, *MNRAS*, 346, 601
- Goto, T., Nichol, R. C., Okamura, S., et al. 2003b *PASJ*, 55, 771
- Goto, T., Okamura, S., Sekiguchi, M., et al. 2003c *PASJ*, 55, 757
- Goto, T., 2003, PhD thesis, astro-ph/0310196
- Haines, C., Mercurio, A., Merluzzi, P., et al. 2004, *A&A* accepted, astro-ph/0403556
- Hamuy, M., Suntzeff, N. B., Heathcote, S. R., et al. 1994, *PASP*, 106, 566
- La Barbera, F., Busarello, G., Merluzzi, P., Massarotti, M., & Capaccioli, M. 2002, *ApJ*, 571, 790
- La Barbera, F., Busarello, G., Massarotti, M., Merluzzi, P., & Mercurio, A. 2003, *A&A*, 409, 21
- Lavery, R. J., & Henry, J. P. 1986, *ApJ*, 304, L5
- Liang, H., Hunstead, R. W., Birkinshaw, M., & Andreani, P. 2000, *ApJ*, 544, 686
- Mercurio, A., Girardi, M., Boschini, W., Merluzzi, P., & Busarello, G. 2003a, *A&A*, 397, 431
- Mercurio, A., Massarotti, M., Merluzzi, P., et al. 2003b, *A&A*, 408, 57
- Merluzzi, P., La Barbera, F., Massarotti, M., Busarello, G., & Capaccioli, M., 2003, *ApJ*, 589, 147
- Morris, S. L., Hutchings, J. B., Carlberg, R. G., et al. 1998, *ApJ*, 507, 84
- Poggianti, B. M. & Barbaro, G. 1996, *A&A*, 317, 379
- Poggianti, B. M., Smail, I., Dressler, A., et al. 1999, *ApJ*, 518, 576
- Poggianti, B. M., Bridges, T. J., Komiyama, Y., et al. 2004, *ApJ*, 601, 197
- Press, W. H., Teukolsky, S. A., Vetterling, W. T., & Flannery, B. P. 1992, in *Numerical Recipes (Second Edition)*, (Cambridge University Press)
- Quintero, A. D., Hogg, D. W., Blanton, M. R., et al. 2003, *ApJ*, 602, 190
- Rizza, E., Burns, J. O., Ledlow, M. J., et al. 1998, *MNRAS*, 301, 328
- Roettiger, K., Burns, J. O., & Loken, C. 1996, *ApJ*, 473, 651
- Salpeter, E. E. 1955, *ApJ*, 121, 161
- Schlegel, D. J., Finkbeiner, D. P., & Davis, M. 1998, *ApJ*, 500, 525

- Shioya, Y., Bekki, K., & Couch, W. 2004, *ApJ*, 601, 654
- Taffoni, G., Mayer, L., Colpi, M. & Governato, F. 2003, *MNRAS*, 341, 434
- Thomas, D., Maraston, C., & Bender, R. 2003, *MNRAS*, 339, 897
- Tomita, A., Nakamura, F. E., Takata, T. et al. 1996, *AJ*, 111, 42
- Trager, S.C., Worthey, G., Faber, S.M., Burstein D., & Gonzalez J.J., 1998, *ApJS*, 116, 1
- van den Berg, S., Pierce, M. J., & Tully, R. B. 1990, *ApJ*, 359, 4
- van den Berg, S. 1991, *PASP*, 103, 390
- van Dokkum, P. G., Franx, M., Kelson, D. D., et al. 1998, *ApJ*, 500, 714
- Worthey, G., Faber, S.M., Gonzalez, J.J., & Burstein, D. 1994, *ApJ*, 94, 687
- Worthey, G., & Ottaviani, D.L. 1997, *ApJS*, 111, 377
- Zabludoff, A. I., Zaritsky, D., Lin, H., et al. 1996, *ApJ*, 466, 104